Mathematical modeling of microbial enhanced oil recovery with focus on bio-plug technology: from the pore to the core scale

David Landa-Marbán

Thesis for the Degree of Philosophiae Doctor (PhD)
University of Bergen, Norway
2019

UNIVERSITY OF BERGEN

Mathematical modeling of microbial enhanced oil recovery with focus on bio-plug technology: from the pore to the core scale

David Landa-Marbán

Thesis for the Degree of Philosophiae Doctor (PhD)
at the University of Bergen

Date of defence: 14.06.2019

Year: 2019

Title: Mathematical modeling of microbial enhanced oil recovery with focus on bio-plug technology: from the pore to the core scale

Name: David Landa-Marbán

Print: Skipnes Kommunikasjon / University of Bergen

Preface

This dissertation is submitted as a partial fulfillment of the requirements for the degree of Doctor Philosophy (PhD) at the University of Bergen. The advisory committee has consisted of Florin Adrian Radu (University of Bergen), Iuliu Sorin Pop (Hasselt University) and Kundan Kumar (Karlstad University).

The PhD project has been financially supported by GOE-IP and the Research Council of Norway through the project IMMENS no. 255426.

Acknowledgements

First of all, I would like to thank my main supervisor Florin. It has been almost 5 years since we started to work together (2 years in Master and 3 years in PhD). I am very grateful for all the guidance, inspiration and discussions at work and also for all the social evenings out in these years. Many thanks to my other two supervisors: Sorin for both guidance of my work and making me feel at home during my three worked visits to Hasselt and Kundan for the corrections and discussions that significantly improved the papers.

My PhD took part of the project "improving microbial selective plugging technology through experimentally based modelling and simulation (IMMENS)". This project was a co-operation between UiB, Uni Research CIPR (NORCE from 2019) and industry partner GOE-IP. Thus, I would like to thank the project leader Gunhild and the researchers who performed the laboratory experiments. Many thanks to Gunhild for all the excellent work as project leader (arranging the yearly work shops, organizing the regular meetings for discussions and for all the questions answered about the details in the experiments). I am really amazed at witnessing Na performing the experiments in the microchannels and perforated domains under the guidance of Tormod, Bartek and Thomas. It has been a pleasure working with Bartek, thanks for the discussions on the core-scale experiments. I would also like to thank Per for his contribution on the sensitivity analysis of the model parameters and both Sarah and Ivar for their contributions in the project meetings.

I have been so lucky for being part of the porous media group in Bergen during my research. Thanks to all the professors, researchers, postdocs and PhDs for the collaborations, especially my friend and office colleague Manuel. I met Manuel when I was writing my master's thesis; we had a couple of academic discussions about my work. Afterwards, we have shared an office during all my PhD. Thanks Manuel for everything. I was fortunate enough to share the office with two more admirable people: Davide and Victor. Thanks for all the nice conversations, especially for our weekly sport's day. Also, thanks to all my close colleagues, a special mention to Manuela, Max, Alessio, Jhabriel and Jakub.

A mis papás, Julia y Daniel, por todo el amor y apoyo que me han brindado en toda mi vida. A mi hermosa familia, Landa Piedra y Marbán Hernández, por todos los momentos juntos. En especial a mi tía Rosario, gracias por todo. A mis amigos en México, en especial Pepo, Yunior, Iván, Brayan, Ricardo, Mayra, Andrea, Gladys, César y Carolina.

Familia y amigos: siempre los llevo en el corazón y siempre son bienvenidos aquí en Noruega.

Jeg gleder meg også til min nye familie som jeg fikk her i Bergen. En spesiell omtale for Osei, Benedicte, Eirik, Veronika, Robert, Birk, Preben, Susann, Maren, Laxzi, Isa og Tor. Tusen takk for alt. Sonia, merci pour tout. Ata, her şey için teşekkürler. Penne and Annelyn, bedankt voor alles. Arooj, ہر چیز کے لیے شکریہ. Shahd, شكرا على كل شيء. Victor, obrigado por tudo. Līga, paldies par visu. Kristina, Дякую за все. Fahim, برای همه چیز ممنونم. Markus, danke mein Freund. Roberta, grazie di tutto. Evelina, ačiū už viską. Tapash and Shifat, সবকিছুর জন্য তোমাকে ধন্যবাদ.

Abstract

This dissertation addresses the applications and challenges of both laboratory experiments and mathematical modeling at different scales, where the main character is biofilm. Thus, the first part of this work shows biological, chemical and physical concepts for the laboratory experiments and mathematical terms for the modeling, upscaling and numerical solutions. The second part contains the research papers.

In our research, we are interested in studying the biofilm to improve the oil extraction. Most of the biofilm models are based on simplifying assumptions, e.g. impermeability, a constant biofilm density and accounting for diffusion but neglecting convection for transport of nutrients. In this work, we propose a pore-scale model for a permeable multi-component biofilm including a variable biofilm density, detachment and transport of nutrients due to convection and diffusion. It is through laboratory experiments that we identify the key processes and variables that need to be considered. Accordingly, we use experimental determined parameters and compute some of the parameters through calibration. In addition, we study the sensitivity of the parameters in the mathematical models.

Pore-scale models are important because they aim to describe physical phenomena in detail and one can derive core-scale models through upscaling. Then, we can reflect the effects of the pore-scale processes on the core scale. Upscaling of pore-scale models allows us to describe the average behavior of a system in an accurate manner with relatively low computational effort. Then, we upscale this pore-scale model in two different geometries: a thin channel and a thin tube, in order to derive one-dimensional effective equations, by investigating the limit as the ratio of the aperture to the length approaches to zero.

In the core-scale laboratory experiments, biofilm is grown in cylindrical cores. Permeability and porosity changes over time at different flow rates and nutrient concentrations are studied. Numerical simulations are performed to compare with the experimental results. We also present how to extend the model to include chemotaxis and interfacial tension reduction due to surface active compounds.

Mathematical models for biofilms are based on coupled non-linear partial differential equations and ordinary differential equations, which may be challenging to solve. Therefore, it is necessary to use advanced numerical methods and simulations to predict the behavior on time of the unknowns in these complex systems. We present some of the common space discretizations, time discretizations and numerical solvers for these

models. We also discuss the difficulty of free boundary problems and the numerical techniques to deal with them. Last but not least, we discuss the challenges of parameter estimation and the application of sensitivity analysis.

Outline

This dissertation consists of two parts. The first part gives an overview of scientific theory and mathematical methods that are relevant to the thesis. The second part contains the research papers.

Part I consists of six chapters. We introduce the concepts related to processes in biofilms, applications of biofilms to real-world problems and the relevance of developing mathematical models in Chapter 1. In Chapter 2 we discuss both laboratory experiments and mathematical models in different geometries at the pore scale. Upscaling techniques to derive effective quantities from the pore to the core scale are discussed in Chapter 3. In Chapter 4 we discuss both laboratory experiments and mathematical models for single- and multi-phase flow at the core scale. The mathematical techniques to solve these models are given in Chapter 5. Finally, a summary of the papers, conclusion and outlook is given in Chapter 6.

Part II contains the scientific results, consisting of the following six papers:

Paper A [56] Landa-Marbán, D., Pop, I. S., Kumar, K., and Radu, F. A. (2019). Numerical simulation of biofilm formation in a microchannel. In Radu, F. A., Kumar, K., Berre, I., Nordbotten, J. M., and Pop, I. S. (editors), *Numerical Mathematics and Advanced Applications ENUMATH 2017*. ENUMATH 2017. Lecture Notes in Computational Science and Engineering, *126*, 799–807. Springer, Cham. doi: 10.1007/978-3-319-96415-7_75.

Paper B [62] Liu, N., Skauge, T., Landa-Marbán, D., Hovland, B., Thorbjørnsen, B., Radu, F. A., Vik, B. F., Baumann, T., and Bødtker, G. (2019). Microfluidic study of effects of flow velocity and nutrient concentration on biofilm accumulation and adhesive strength in the flowing and no-flowing microchannels. *Journal of Industrial Microbiology & Biotechnology*. doi: 10.1007/s10295-019-02161-x.

Paper C [55] Landa-Marbán, D., Liu, N., Pop, I. S., Kumar, K., Pettersson, P., Bødtker, G., Skauge, T., and Radu, F. A. (2019). A pore-scale model for permeable biofilm: Numerical simulations and labora-

tory experiments. *Transport in Porous Media*. *127*(3), 643–660. doi: 10.1007/s11242-018-1218-8.

Paper D Landa-Marbán, D., Bødtker, G., Kumar, K., Pop, I. S., and Radu, F. A. (2019). An upscaled model for permeable biofilm in a thin channel and tube. In review.

Paper E D. Landa-Marbán, D., Bødtker, G., Kumar, K., Pettersson, P., Pop, I. S., Vik, B. F., and Radu, F. A. (2019). Mathematical modeling of bioplug technology: Laboratory experiments and numerical simulations. In preparation.

Paper F [57] Landa-Marbán, D., Radu, F. A., and Nordbotten, J. M. (2017). Modeling and simulation of microbial enhanced oil recovery including interfacial area. *Transport in Porous Media 120*(2), 395–413. doi: 10.1007/s11242-017-0929-6.
Paper based on work from master's thesis [54].

Contents

Part I

Scientific Background

Chapter 1

Introduction

The art of mathematical modeling consists of describing systems with enough complexity to predict its behavior, but simple enough to have as less number of parameters as possible. Mathematical models have been used to solve real world problems in different areas, such as medicine, engineering, biology and geophysics. In this work we are interested in mathematical models at different scales of bacterial effects for improving the oil recovery. Different types of bacteria are used in specific applications. Despite the ubiquitous presence of bacteria, a lot remains unknown about them. For example, even now, scientists do not agree about the estimation of how many different bacteria species exists. Amman and Rosselló-Móra [5] states that only millions of species exist instead of previous estimates of billions. Today, the physiology of more than 30,000 formally named species in pure culture have been investigated [31]. In recent years, industrial applications of bacteria has increased significantly. This thesis develops mathematical and computational tools to study one of the important applications, that is using them to enhance the oil recovery (microbial enhanced oil recovery, MEOR).

Novel mathematical models for MEOR must be built to improve accuracy and enhance confidence in numerical results. In this work, we refer to the pore scale (also known as micro scale) to the size of micrometers to millimeters and to the core scale (also known as Darcy scale or macro scale) from order of centimeters to meters. This thesis aims to describe the methodology to derive core-scale models from experimental-based pore-scale modeling through homogenization.

The main contributions of this thesis are:

1. **A novel pore-scale model for a permeable multi-component biofilm.** The proposed mathematical model includes a variable biofilm density, detachment of biofilm components due to erosion and transport of nutrients by convection and diffusion. The model development is performed in close relationship with the physical experimental observations. This mathematical model is built in a thin channel as shown in Paper A, where we present the algorithm to solve it numerically. The laboratory experiments which inspired this model are presented in Paper B. The formulation of this mathematical model in a perforated domain is presented

in Section 2.2.

2. **Experimental determined parameters for the pore-scale mathematical model.** From the laboratory experiments the dimensions of the channel, the injected nutrient concentration and the flow velocity are known. The coverage biofilm area is measured over time for different flux velocities. Using the best parameter model estimates reported in literature, we calibrate the stress coefficient to fit the measurements of coverage biofilm area over time for four different flux velocities. A detailed discussion of the model calibration is presented in Paper C. To identify the model parameters that may be estimated with relatively less accuracy, and the ones requiring a more accurate estimation, we performed a global sensitivity analysis.

3. **Upscaling the pore-scale model in two different pore geometries.** The full model including all processes from the pore scale to the core scale is generally too complex to be solved; therefore, homogenization is used to derive core-scale models which represent the effective behavior of the system. Details on the mathematical techniques to upscale the model in a thin cylinder and channel are shown in Paper D. In addition, numerical computations of the effective models and a comparison with a well-known core-scale model are presented.

4. **Comparison of core-scale experiments with numerical simulations.** Laboratory experiments were performed in core samples to study the changes of permeability and porosity over time due to biofilm formation at different flux velocities. From the laboratory experiments the dimensions of the core, the flux velocity, injected nutrient concentration and initial porosity, volume fraction of biofilm and permeability are known. Laboratory results and numerical simulations are presented in Paper E. The stress coefficient is calibrated to fit the measurements of permeability reduction due to biofilm growth. Numerical simulations of a two-phase core-scale model containing more complex processes are presented in Paper F.

1.1 Biofilm

The systems that we are interested in modeling are biofilms. Vu et al. [101] defines a biofilm as an aggregation of bacteria, algae, fungi and protozoa (microbes) enclosed in a matrix consisting of a mixture of polymeric compounds, primarily polysaccharides, generally referred to as extracellular polymeric substance (EPS). Bacteria have different shapes and sizes, typically of the order of micrometers. Intuitively, we can imagine the EPS as the "house" of the bacteria. Jefferson [45] mentioned four potential incentives behind the formation of biofilms: protection from harmful conditions (defense), sequestration to a nutrient-rich area (colonization), utilization of cooperative benefits (community) and biofilms as the default mode of growth (reproduction). A herd of land

animals, flock of birds, swarming of insects, shoal of fish and community of humans are other examples of living organisms who come together for beneficial purposes.

Toyofuko et al. [97] describes biofilm formation through three steps: planktonic cell attachment to the surface, formation of a structured architecture with the assistance of EPS in the maturation stage and cells leaving the biofilm in the dispersal stage. Different environmental factors affect the biofilm, such as temperature and pH.

Biofilms are complex systems, involving different physical, chemical and biological processes. Some of the relevant processes in biofilms include the following:

- Flow: Movement of a fluid (e.g. water) is produced by pressure gradient [6].
- Transport: Bacteria and nutrients are driven by the combined effects of diffusion (from concentration gradients) and convection (from bulk fluid flow) [12].
- Attachment: The tendency of bacteria to adhere to surfaces [104].
- Bacterial decay: Death of the bacterial population [14].
- Nutrient consumption: Bacteria require nutrients for growth, reproduction, formation of bioproducts and movement. Generally we distinguish two scenarios: one in which the nutrients are abundant and the other in which they are limiting. [91].
- Bacterial reproduction: Bacteria in a suitable medium can increase in number by first having each cell increase in size and then each cell divides to produce two daughter cells [87].
- Endogeneous respiration: Process by which microorganisms consume cell reserves in the absence of substrate and thereby continue to use a terminal electron acceptor [67]. Electron acceptors are ions or molecules that act as oxidizing agents in chemical reactions.
- Erosion: Removal of the small groups of cells from the surface of the biofilm caused by shear forces of the moving fluid in contact with the biofilm surface [66].
- Abrasion: Removal of small groups of cells from the surface of the biofilm caused by the collision of biofilm support particles, e.g. during backwashing of fixed bed reactors [66].
- Sloughing: An event where large amounts or entire sections of biofilm leave a support surface and enter the sourronding media [9].
- Formation of bioproducts: Microbial activity produces biomass, acids, gases, polymers, solvents and biosurfactants [90].
- Quorum sensing: Cell-to-cell communication between bacteria mediated by small diffusible signal molecules that trigger changes in gene expression in response to fluctuations in population density [7].
- Taxis: Preferential migration of a cell due to a gradient of some factor in the environment [13]. Taxis have been observed in response to many different types of environmental stimuli such as metabolites and signalling molecules, temperature, light, salinity, oxygen, the magnetic field and pH [51].

It is worth to mention that not all of the aforementioned processes are relevant for cer-

tain applications. Depending on the problem, diverse mathematical models can be build including one or several of these processes.

Table 1.1 shows both beneficial applications and negative effects of biofilms.

1.2 Microbial enhanced oil recovery

Microbial enhanced oil recovery (MEOR) is an enhanced oil recovery method relying on microorganisms and their metabolic products to mobilize residual oil in a cost-effective and eco-friendly manner. The first MEOR field test was reported from the Lisbon field, Union County, Arkansas, USA in 1954 [108]. Since then, the interest in this technology has increased and a lot of research has been done for industrial applications. A recent review of MEOR methods can be found in [106].

In the previous section we mentioned that biofilms produce biomass, acids, gases, polymers, solvents and biosurfactants. Bryant and Lockhart [20] summarize the effects of these bioproducts on enhanced oil recovery (EOR):

- Biomass: Selective and non-selective plugging, emulsification through adhesion to oil, changing wettability of mineral surfaces, desulfurification of oil and reduction of oil viscosity and pour point.
- Acids: Produce CO_2 through reaction with carbonate minerals and increase rock porosity and permeability.
- Gases: Reservoir repressurization, oil swelling, viscosity reduction and increased permeability caused by solubilization of carbonate rocks.
- Solvents: Dissolution of oil.
- Surfactants: Lowering interfacial tension and emulsification.
- Polymers: Mobility control and selective or non-selective plugging.

Fig. 1.1 shows the different effects of bacteria for EOR.

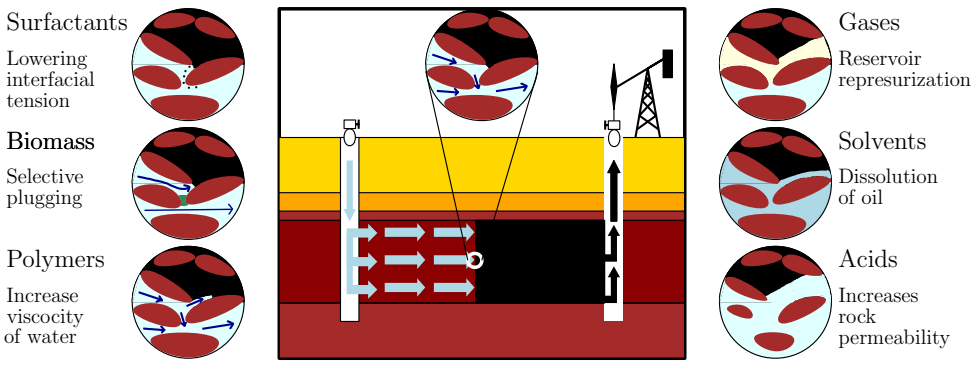

Figure 1.1: Effects of bioproducts in a reservoir to EOR.

Table 1.1: *Examples of biofilm species for industrial applications and causing negative effects*

Beneficial biofilm	Description	Species example
Bioremedation	To detoxify contaminants in the soil and other environments, e.g., oil spills.	*Aeromicrobium erythreum* [22]
Bioleaching	A simple and effective technology for metal extraction from low-grade ores and mineral concentrates.	*Acidithiobacillus thiooxidans* [27]
Water treatment	Improving the quality of water to make it more acceptable for a specific purpose.	*Nitrosomonas europaea* [82]
Microbial enhanced oil recovery (MEOR)	Process of recovering oil not already extracted from an oil reservoir through primary or secondary recovery techniques.	*Clostridium tryobutyricum* [69]
Biofuel cell	A bioelectrochemical energy system capable of converting chemical energy available in organic substrates into electrical energy using bacteria as a biocatalyst to oxidize the biodegradable substrates.	*Pseudomonas aeruginosa* [49]
Detrimental biofilm	**Description**	**Species example**
Medical devices	Biofilm formation on medical devices is associated with hospital acquired infections.	*Pseudomonas aeruginosa* [80]
Biofouling	The unwanted growth of marine organisms on stationary, submerged equipment.	*Leucothrix mucor* [109]
Chronic infections	When bacteria succeed in forming a biofilm within the human host, the infection often turns out to be untreatable and will develop into a chronic state.	*Legionella pneumophila* [15]
Dental plate	Biofilm that grows on surfaces within the mouth causing dental decay and gum disease.	*Streptococcus mutans* [64]
Biodeterioration	Changes in the quality or value of a material, which make it less functional in utilization terms, e.g., pieces in museums.	*Aspergillus* [70]

1.3 The importance of mathematical modeling

A mathematical model is a simplified representation of certain aspects of a real system that uses mathematical language to describe its behavior; and so studying the effects of different components and making predictions about behavior. Carrera [21] proposed the scheme in Fig. 1.2 to summarize the process of mathematical modeling of systems when computational schemes are the desired result. From this Figure we observe a cycle in the process, meaning that if the agreement between predictions and observations is less than desirable, it is necessary to re-enter the modeling cycle again.

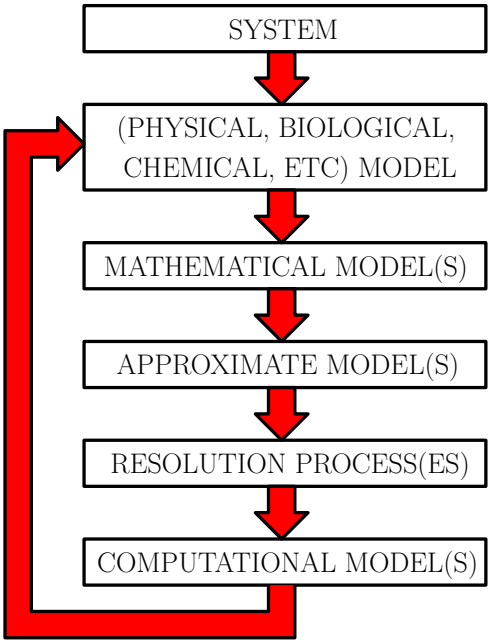

Figure 1.2: Scheme of the process of mathematical modeling. Figure adapted from [21]

Mathematical models in MEOR are important as they help to predict the applicability of an MEOR strategy and to optimize the benefits. Modeling of biofilm started in the early 1980s [102]. Horn and Lackner [43] give a review of the evolution of modeling of biofilm systems during the last three decades. The authors concluded that even though these models have allowed us to understand some processes in biofilms, the measurement of the input parameters needs to improve and current biofilm models should include mechanical properties of biofilms.

On the other hand, we can find many mathematical models for biofilms in literature. However, most of the existing biofilm models neglect important processes and aspects in biofilm systems, e.g., permeability of biofilms [4, 29], biofilm components (e.g., EPS and water) [26, 100] and detachment [23, 103]. Therefore, novel mathematical models must be built to improve accuracy and enhance confidence in numerical results.

Chapter 2

Pore-scale modeling

The pore size in a core sample from a reservoir is of the order of μm [76]. Physical phenomena such as interfaces between the fluid and biofilm, attachment of the bacteria to the pore walls and detachment of biomass can be observed in more detail at this scale. Pore-scale experiments can be designed to estimate model parameters of these phenomena that can be used in core-scale models after deriving effective quantities through upscaling. In this Chapter we describe laboratory experiments and mathematical models to study the biofilm formation in both microchannels and micromodels.

2.1 Microchannels

Laboratory experiments are performed in different systems, such as microchannels. Usually these microchannels have a depth much smaller than the width and length, allowing us to model the system in two dimensions.

2.1.1 Laboratory experiments

In this project a glass micromodel (Micronit, Netherland), a camera (VisiCam 5.0) and two syringe pumps (NE-1000 Series, Syringe Pumps) were used to perform the experiments. The bacterium *Thalassospira* strain A216101 was used for the laboratory studies, which is facultative anaerobic and uses nitrate as alternative finale electron acceptor. Pyruvate was added as a carbon source to a marine mineral medium to produce different nutrient concentrations. Biofilm growth was established in the micromodel by first adding bacteria (inoculation) and then flooding with nutrient medium at different flow rates and nutrient concentrations. The micromodel used in the laboratory has a width of 100 μm and thickness/depth of 20 μm. Fig. 2.1 shows the microchannel before and after inoculation. First, microbes and nutrients were injected in the vertical channel for 24 h at a rate of 1 μl/min. Afterwards, the whole system was closed for one day to allow the suspended bacteria to attach themselves to the surface. Then, we started to inject nutrients from the left channel at different flow rates and nutrient concentrations. Bacterial

sloughing was not observed during the time the experiments were performed (6-7 days). A detailed description of the performed experiments can be found in Paper B.

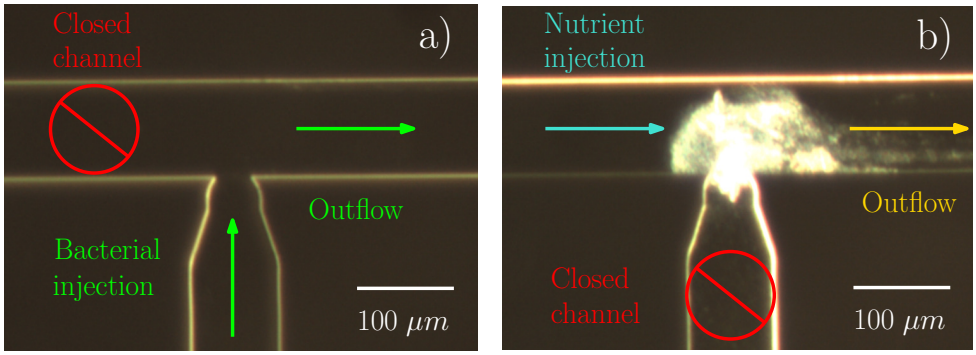

Figure 2.1: Microchannel before and after inoculation. Bacteria was injected first through the vertical channel (a). Nutrients were injected through the left channel for some days (b). Photographed by Na Liu.

2.1.2 Mathematical modeling

We mentioned before that biofilm are complex systems involving different processes. It is important to point out that several magnitudes of difference on time scale among these processes exist (see Table 2.1).

Table 2.1: *Time scale magnitudes for different processes related to biofilms [43]*

Process	Time scale	Process	Time scale
Advection	10^{-2} s – 10^{-1} s	Biomass growth	10^{5} s
Diffusion	10^{3} s	Erosion	10 s
Substrate conversion	10^{-1} s – 10^{2} s	Sloughing	10^{5} s

According to the application, we use different approaches to model biofilms. Cellular automata (CA) are examples of discrete mathematical systems constructed from many identical components, each simple, but together capable of complex behaviour [105]. CA-based biofilm models have been developed in previous years [83]. One of the disadvantages of these models is that they do not adress some relevant physical processes such as deformation by shear forces [43]. Multidimensional continuum models are based on physical law equations (e.g., conservation of mass). These models have been applied to biofilms and can handle more physical processes than CA. Alpkvist and Klapper [4] built a multidimensional multispecies continuum model for heterogeneous biofilm. Duddu et al. [29] built a mathematical model including shear forces caused by water flux. van Noorden et al. [100] built a mathematical model for biofilm formation in a thin strip. Following the same ideas, in Papers A and C we developed a pore-scale model for biofilm

formation in a thin strip geometry. We refer to these papers for details on the formulation of the mathematical model in this geometry.

2.2 Micromodels

A more general geometry than microchannels consists of a perforated domain with void spaces known as micromodels. Researchers have used micromodels to study diverse biofilm processes for different grain geometries, i.e. circles [98], triangles [50] and polygons [48]. Nambi et al. [71] used micromodels to determine how flow hydrodynamics and mass transfer limitations along a transverse mixing zone affect biomass growth. Karambeigi et al. [48] performed experiments in micromodels to study the potential of bioplugging of high permeable layers of porous media. Likewise, scientists have developed and implemented mathematical models in this geometry, e.g., Deng et al. [26] studied numerically the effects of permeable biofilm in a perforated domain. Therefore, there is an increased need for novel mathematical models to investigate the mechanisms of biofilm development in different pore structures, like micromodels.

2.2.1 Laboratory experiments

Micromodels are used to study the effects of biomass on bioplugging. Fig. 2.2 shows a picture of a micromodel with biofilm. To study the permeability reduction and flow diversion at different nutrient concentrations and flow rates, experiments in microchannels were performed in our project. The average velocity in the pore is of order of mm/s and the porosity is about 0.4.

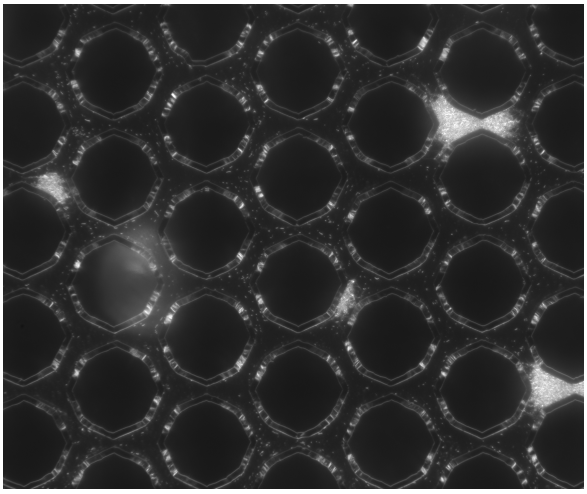

Figure 2.2: Biofilm growth in a micromodel. Photographed by Na Liu.

Karambeigi et al. [48] performed laboratory experiments in a micromodel with two layers of low and high permeable zones to study the oil recovery using bio plugging. After

image analysis, the authors reported an increased of oil recovery of approximately 40 %.

2.2.2 Mathematical modeling

In this subsection we write mathematical equations for a 2D perforated pore-scale domain. As in Paper C, we assume that the biofilm consists of four components: water, EPS, active bacteria and dead bacteria. Moreover, we assume that the fluid flow and nutrients are in a steady state when we compute the biofilm growth potential and volume fractions at each time step, the biofilm growth occurs in the pore walls, there is only one nutrient, which is mobile both in the water and biofilm, the temperature is constant and the gravity effects are neglected.

2.2.2.1 Geometrical settings

Fig. 2.3 shows the water domain, biofilm domain, solid domain and all boundaries in the perforated domain.

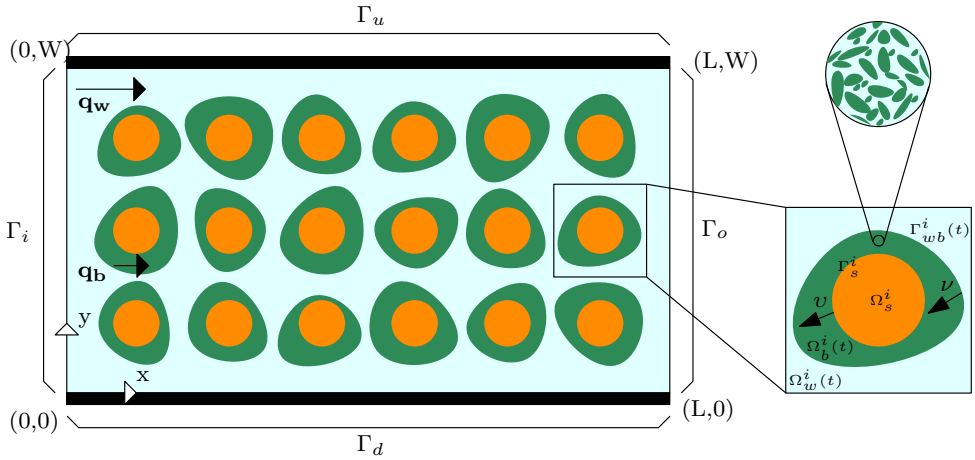

Figure 2.3: Schematic representation of the porous medium.

We consider a two-dimensional domain of length L and width W:

$$\Omega := (0, L) \times (0, W).$$

The boundary of the domain consists of the upper and lower walls, the inflow and the outflow:

$$\Gamma_u := [0, L] \times \{W\}, \quad \Gamma_d := [0, L] \times \{0\}, \quad \Gamma_i := \{0\} \times [0, W], \quad \Gamma_o := \{L\} \times [0, W].$$

The domain is perforated, consisting of a pore space filled with water $\Omega_w(t)$, solid grains Ω_s and biofilm attached to the grains $\Omega_b(t)$. For ease of the presentation, we assume that there is no biofilm formation on the domain walls. We denote the water-biofilm

interfaces by $\Gamma_{wb}(t)$ and the solid grain boundary by Γ_s. We note that both domains $\Omega_w(t)$ and $\Omega_b(t)$ and interface $\Gamma_{wb}(t)$ changes over time due to biofilm growth, bacterial decay and detachment.

2.2.2.2 Equations in the water phase

In the water phase $\Omega_w(t)$, equations to describe the water flux and transport of nutrients are needed. Assuming that water is incompressible, the water flow is described by the conservation of mass and Stokes equation

$$\nabla \cdot \boldsymbol{q}_w = 0, \quad \mu \Delta \boldsymbol{q}_w = \nabla p_w,$$

where μ is the water viscosity, p_w is the water pressure and $\boldsymbol{q}_w = (q_w^{(1)}, q_w^{(2)})$ is the water velocity.

To model the transport of nutrients in the micromodel, denoting by D the scalar diffusion of nutrients, the nutrient concentration in the water (c_w) satisfies the convection-diffusion equations

$$\partial_t c_w + \nabla \cdot \boldsymbol{J}_w = 0, \quad \boldsymbol{J}_w = -D\nabla c_w + \boldsymbol{q}_w c_w,$$

where $\boldsymbol{J}_w$ is the nutrient flux in water. To include nutrient dispersion in the model, the scalar diffusion D can be replaced by a tensor depending also on the water velocity. To incorporate the transport of bacteria in the water phase, we can add extra convection-diffusion equations with their corresponding diffusion (or dispersion) expressions.

2.2.2.3 Equations in the biofilm phase

As mentioned before, the biofilm components are water, EPS, active bacteria and dead bacteria ($j = \{w, e, a, d\}$). Let $\theta_j(t, \boldsymbol{x})$ and $\rho_j(t, \boldsymbol{x})$ denote the volume fraction and the density (relative to volume fraction) of species j at time t and position $\boldsymbol{x}$, respectively. The biomass and water are assumed incompressible ($\rho_j(t, \boldsymbol{x}) = \rho_j$). The volume fractions are constrained to

$$\sum_j \theta_j(t, \boldsymbol{x}) = 1. \tag{2.1}$$

In the biofilm, the biomass can increase or decrease due to EPS production, bacterial reproduction and bacterial decay. Let $\boldsymbol{u}$ be the velocity of the biomass. Assuming that the biofilm growth is irrotational [29], we can derive the velocity field from a function potential Φ,

$$\boldsymbol{u} = -\nabla \Phi.$$

Recalling that biofilms are mostly water, we assume that the water content is constant ($\partial_t \theta_w = 0$). Without this assumption, an extra expression for the water content would be necessary to have as many equations as variables.

We describe the water flux in the biofilm by the mass conservation and the Brinkman equation

$$\nabla \cdot \boldsymbol{q}_b = 0, \quad \frac{\mu}{\theta_w} \Delta \boldsymbol{q}_b - \frac{\mu}{k} \boldsymbol{q}_b = \nabla p_b, \tag{2.2}$$

where $\boldsymbol{q}_b$ and p_b are the velocity and pressure of the water in the biofilm, respectively and k is the biofilm permeability.

Inside the biofilm, the nutrients are dissolved in the water. The nutrient concentrations satisfy the following convection-diffusion-reaction equations:

$$\partial_t(\theta_w c_b) + \nabla \cdot \boldsymbol{J}_b = R_b, \quad \boldsymbol{J}_b = -\theta_w D \nabla c_b + \boldsymbol{q}_b c_b,$$

where c_b, $\boldsymbol{J}_b$ and $R_b$are the nutrient concentration, flux in the biofilm and reaction term given by

$$R_b = -\mu_n \theta_a \rho_a \frac{c_b}{k_n + c_b},$$

where μ_n is the maximum rate of nutrient utilization and k_n is the Monod-half velocity coefficient.

The conservation of mass for the biomass components ($l = \{e, a, d\}$) is given by

$$\partial_t(\rho_l \theta_l) + \nabla \cdot (\boldsymbol{u} \rho_l \theta_l) = R_l, \tag{2.3}$$

where R_l are the reaction rates for the volume fractions

$$\begin{aligned}
R_b &= -\mu_n \theta_a \rho_a \frac{c_b}{k_n + c_b}, \\
R_e &= Y_e \mu_n \theta_a \rho_a \frac{c_b}{k_n + c_b}, \\
R_a &= Y_a \mu_n \theta_a \rho_a \frac{c_b}{k_n + c_b} - k_{\text{res}} \theta_a \rho_a, \\
R_d &= k_{\text{res}} \theta_a \rho_a,
\end{aligned}$$

where Y_e and Y_a are yield coefficients and k_{res} is the bacterial decay rate. Then, the included processes are bacterial reproduction, production of EPS and death of bacteria. The yield coefficients allow us to include in the model the produced amount of bacteria or metabolites given the consumed nutrients, fulfilling $\sum_k Y_k \leq 1$.

Following [4], summing Eq. 2.3 over l and using Eq. 2.1, since θ_w and ρ_l (for all l) are constants, the growth velocity potential satisfies

$$-\nabla^2 \Phi = (1 - \theta_w)^{-1} \sum_l \frac{R_l}{\rho_l}.$$

Once we have introduced the model equations in the water and biofilm phases, we need to provide appropriate coupling conditions in the biofilm-water interfaces.

2.2.2.4 Equations at the biofilm-water interface

Assuming that the normal velocity of the interface between the biofilm and fluid is negligible with respect to the velocity of the fluid phase, we choose natural interface conditions, that is, the continuity of velocity and that of the normal component of the stress tensor across the interface [30]

$$\boldsymbol{q}_w = \boldsymbol{q}_b, \quad \boldsymbol{\nu} \cdot (\mu \nabla \boldsymbol{q}_w - \mathbb{1} p_w) = \boldsymbol{\nu} \cdot ((\mu/\theta_w) \nabla \boldsymbol{q}_b - \mathbb{1} p_b).$$

Conservation of nutrients is ensured by the Rankine-Hugoniot condition,

$$(\boldsymbol{J}_b - \boldsymbol{J}_w) \cdot \boldsymbol{\nu} = v_n(\theta_w c_b - c_w).$$

The nutrient concentration is assumed to be continuous across the interface,

$$\theta_w c_b = c_w.$$

We set the growth velocity potential at the interface to zero,

$$\Phi = 0.$$

Homogeneous Neumann conditions are considered for the biomass components,

$$\boldsymbol{\nu} \cdot \nabla \theta_l = 0.$$

The location of the interface $\Gamma_{wb}(t)$ changes in time due to the EPS production,bacterial reproduction, bacterial decay and shear stress produced by the water flux. To incorporate this, we follow [95] and [100] and use the following definition for the tangential shear stress:

$$S = ||(\mathbb{1} - \boldsymbol{\nu}\boldsymbol{\nu}^T)\mu(\nabla \boldsymbol{q}_w + \nabla \boldsymbol{q}_w^T)\boldsymbol{\nu}||,$$

where $\|\cdot\|$ denotes the maximum norm. Then, the normal velocity of the interface is given by

$$v_n = \boldsymbol{\nu} \cdot \boldsymbol{u} + k_{str} S$$

where k_{srt} is a constant for the shear stress.

The water-biofilm interface $\Gamma_{wb}(t)$ and the solid grain boundary Γ_s can be described as zero sets of appropriate level-set functions. In Section 5.2 we discuss about free boundary problems and three different approaches for mathematical modeling. In Papers A, C and D the arbitrary Lagrangian-Eulerian method was used to track the free boundary. However, for a perforated domain we use a different method. The level set method tracks the position of the water-biofilm interface over time. The level set approach for modeling processes involving free boundaries at the pore scale was introduced by van Noorden [99]. Following [88], the water-biofilm interface $\Gamma_{wb}(t)$ and the solid interface Γ_s can be described as zero sets of appropriate level-set functions $L : \Omega \times (0, T] \to \Re$ and $S : \Omega \to \Re$:

$$\Gamma_{wb}(t) = \{\boldsymbol{x} \in \Omega |\ L(\boldsymbol{x}, t) = 0\} \quad \text{and} \quad \Gamma_s = \{\boldsymbol{x} \in \Omega |\ S(\boldsymbol{x}) = 0\} \tag{2.4}$$

Then the water, biofilm and solid domains can be written as

$$\Omega_w(t) = \{\boldsymbol{x} \in \Omega | L(\boldsymbol{x}, t) < 0 \text{ and } S(\boldsymbol{x}) < 0\}, \tag{2.5}$$

$$\Omega_b(t) = \{\boldsymbol{x} \in \Omega | L(\boldsymbol{x}, t) > 0 \text{ and } S(\boldsymbol{x}) < 0\}, \tag{2.6}$$

$$\Omega_s = \{\boldsymbol{x} \in \Omega | L(\boldsymbol{x}, t) > 0 \text{ and } S(\boldsymbol{x}) > 0\}. \tag{2.7}$$

We need an extra equation to describe the evolution in time of the level-set function L. This function satisfies

$$\partial_t L + v_n |\nabla L| = 0. \tag{2.8}$$

An extended discussion of the level set method is given in Section 5.2.

Boundary and initial conditions are needed to close the system of equations and to have a unique solution. As water is injected, we need to specify either the flux or the pressure at the inflow and outflow. The injected nutrient concentration is kept constant during the experiments; therefore, the nutrient concentration at the inflow is given. The upper and lower boundaries are closed; hence no slip boundary condition for the water flow and no flux condition for the nutrients are considered on these boundaries. For the level set function, homogeneous Neumann conditions are considered.

The previous mathematical model can be calibrated against laboratory experiments and implemented for simulations. Implementation of mathematical model equations with free boundaries is quite challenging, as it requires the numerical solution of coupled partial differential equations in a changing domain. In Chapter 5 we discuss numerical solutions of these mathematical models.

Chapter 3

Upscaling

Upscaling from pore scale to core scale allows us to describe the average behavior of the system in an accurate manner with relatively low computational effort compared to fully detailed calculations starting at the microscale and to determine constitutive relationships. The goals of homogenization are to extract effective or homogenized parameters for heterogeneus media and to derive simpler macroscopic models from complex microscopic models. Recent works have been done to derive upscaled models, e.g., Neuweiler and Vogel [72] derived effective parameters upscaling unsaturated flow in heterogeneous porosu media, Peszynska et al. [81] built and upscaled a mathematical model for biofilm growth using imaging and experiments, Brun et al. [19] derived thermal Biot equations throught upscaling a fluid-structure model at the microscale and Schulz [88] derived an effective model for permeable biofilm in a perforated porous medium saturated by water. Fig 3.1 shows experiments and models for biofilm at different scales. We point out the differences in order of magnitude on the time when experiments are performed at different scales. While experiments in micromodels are performed for weeks, the time extraction in reservoirs could last for many years.

3.1 Non-dimensional equations

The first step in the upscaling process is to identify and separate the different scales. In the microchannel model presented in Paper C, we can distinguish between the length and width of the microchannel. In the perforated domain presented in Section 2, we can distinguish between the dimensions of the micromodel and the dimensions of the grains. One of the aims of writing a mathematical model in a dimensionless form is to show the temporal and spatial scale that the terms depend on. To make a dimensionless dimensionless, reference values are introduced. We focus on the pore-scale model in Section 2. In this aim, we introduce the reference time T, length (domain) L, length (grains) l, water velocity $Q := L/T$, biomass velocity U, pressure P and concentration C. The perforated domain is characterized by the ratio between the reference length of the grains and the reference length of the domain $\varepsilon := l/L$, which is called the dimensionless

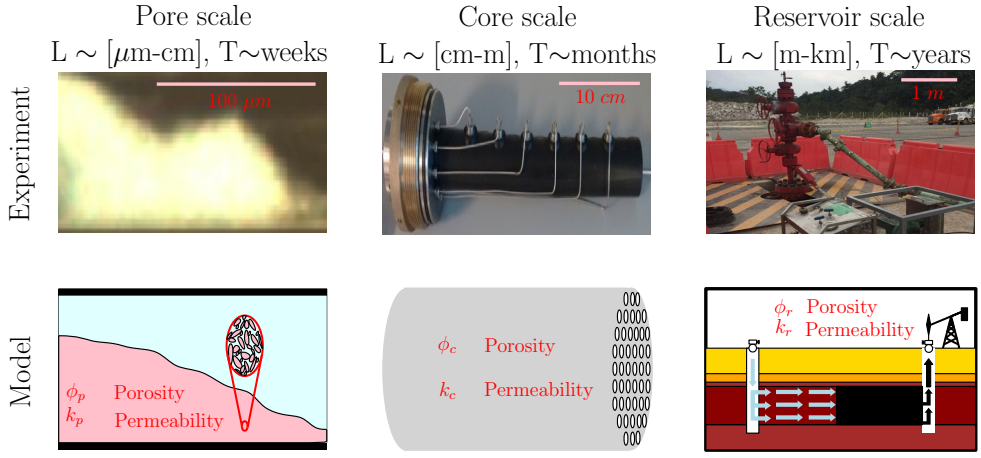

Figure 3.1: Experiments and models of biofilm formation at different scales. Photographed by Na Liu (pore-scale experiment), Bartek Vik (core-scale experiment) and both Alejandro Contreras and David Bautista (reservoir-scale experiment).

aspect ratio. Then, we define dimensionless coordinates $\boldsymbol{x}' := \boldsymbol{x}/L$ and time $t' := t/T$.

We define the following dimensionless parameters

$$P_e := \frac{QL}{D}, \quad D_a := T\mu_n, \quad k_n' := \frac{k_n}{C}, \quad k' := \frac{k}{\epsilon^2 l^2}, \quad \mu' := \frac{\mu Q}{\epsilon^2 PL},$$
$$k_{str}' := \frac{Pk_{str}}{U}, \quad k_{res}' := Tk_{res}.$$

We observe that the viscosity and permeability are scaled with ϵ^2. The reason for this upscaling is that the new dimensionless viscosity balances the friction of the fluid on the interface and the ratio between viscocity and permeability should be independent of ϵ [88].

Let us consider the conservation of mass and Brinkman equation (2.2). The non-dimensional unknowns are given by

$$\boldsymbol{q}_b' = (q_{b,x'}', q_{b,y'}') := \frac{\boldsymbol{q}_b}{Q}, \qquad p_b' := \frac{p_b}{P}$$

Then, the dimensionless form of these equations is given by:

$$\partial_{x'} q_{b,x'}' + \partial_{y'} q_{b,y'}' = 0,$$
$$\frac{\mu'\epsilon^2}{\theta_w}(\partial_{x'}^2 q_{b,y'}' + \partial_{y'}^2 q_{b,y'}') - \frac{\mu'}{k'} q_{b,y'}' = \partial_{y'} p_b,$$
$$\frac{\mu'\epsilon^2}{\theta_w}(\partial_{x'}^2 q_{b,x'}' + \partial_{y'}^2 q_{b,x'}') - \frac{\mu'}{k'} q_{b,x'}' = \partial_{x'} p_b$$

Using the previous references values and dimensionless parameters, the non-dimensional model for the remaining equations in pore-scale model introduced in Section 2 can be obtained.

P_e is known as the Péclet number and expresses the ratio of a diffusive time scale and the transport time scale, while D_a is known as the Damköhler number and expresses the ratio between the diffusion and the reaction time scale. In Paper D we assume that these both numbers do not depend on the aspect ratio of the pores, i.e., these numbers are $O(1)$ in ϵ. Other regimes where transport or reaction dominate diffusion are of certain interest and lead to different effective models. Investigating such cases is part of the future work.

3.2 Homogenization

Once a mathematical model is brought to a dimensionless formulation, we can upscale the model applying homogenization. Homogenization is a mathematical tool for upscaling models posed in a complex domain or involving rapid oscillatory characteristics. We refer to [8, 24, 44] for a detailed description of homogenization techniques.

We consider a domain $\Omega \subset \mathfrak{R}^d$ with boundary denoted by $\partial\Omega$. Furthermore, we consider the 2D case ($d = 2$), where we denote the flux vector as $\boldsymbol{q}^\epsilon(\boldsymbol{x})$. The asymptotic expansion method assumes the existence of two scales: a fast scale used for the rapidly oscillating characteristics and a slow scale used for the average behavior of the system. Using the homogenization ansatz, the flux $\boldsymbol{q}$ can be expanded asymptotically as

$$\boldsymbol{q}^\epsilon(\boldsymbol{x}) = \sum_{k=0}^{\infty} \epsilon^k \boldsymbol{q}_k(\boldsymbol{x}, \boldsymbol{y}) = \boldsymbol{q}_0(\boldsymbol{x}, \boldsymbol{y}) + \epsilon \boldsymbol{q}_1(\boldsymbol{x}, \boldsymbol{y}) + \dots, \tag{3.1}$$

where the vector $\boldsymbol{y}$ is defined as

$$\boldsymbol{y} = \frac{\boldsymbol{x}}{\epsilon}. \tag{3.2}$$

Let $Y = [0, 1] \times [0, 1]$ denote the closed unit cube. The functions $\boldsymbol{q}_k$ are assumed to be Y-periodic

$$\boldsymbol{q}_k(\boldsymbol{x}, y_1, y_2) = \boldsymbol{q}_k(\boldsymbol{x}, y_1 + 1, y_2) = \boldsymbol{q}_k(\boldsymbol{x}, y_1, y_2 + 1) \tag{3.3}$$

and all have an order of magnitude not depending on ϵ. These assumptions lead the flux factors $\boldsymbol{q}_k$ depend on two variables: the slow variable $\boldsymbol{x}$ and the fast variable $\boldsymbol{y}$. The fast variable $\boldsymbol{y}$ transfers the rapid oscillations at the micro-scale ($O(\epsilon)$) to the macro-scale ($O(1)$), while the average behavior of the system is described by the slow variable $\boldsymbol{x}$. Periodicity is assumed for the ease of presentation.

The asymptotic assumption on $\boldsymbol{q}(\boldsymbol{x})$ brings different functions $\hat{\boldsymbol{q}}_k(\boldsymbol{x}) = \boldsymbol{q}_k\left(\boldsymbol{x}, \frac{\boldsymbol{x}}{\epsilon}\right)$, leading to changes in the derivatives. For example, the gradient of the x_1 component of the flux $\boldsymbol{q}_k(\boldsymbol{x}, \boldsymbol{y})$ is given by

$$\frac{\partial \hat{q}_k^1}{\partial x_i}(\boldsymbol{x}) = \frac{d q_k^1}{d x_i}\left(\boldsymbol{x}, \frac{\boldsymbol{x}}{\epsilon}\right) = \frac{\partial q_k^1}{\partial x_i}(\boldsymbol{x}, \boldsymbol{y}) + \frac{\partial y_i}{\partial x_i}\frac{\partial q_k^1}{\partial y_i}(\boldsymbol{x}, \boldsymbol{y}) = \frac{\partial q_k^1}{\partial x_i}(\boldsymbol{x}, \boldsymbol{y}) + \frac{1}{\epsilon}\frac{\partial q_k^1}{\partial y_i}(\boldsymbol{x}, \boldsymbol{y}). \tag{3.4}$$

In this way, the vector differential operator is given by

$$\nabla \to \nabla_x + \frac{1}{\epsilon}\nabla_y \tag{3.5}$$

and the Laplacian operator by

$$\Delta \to \Delta_x + \frac{1}{\epsilon}\Big(\nabla_x \cdot \nabla_y + \nabla_y \cdot \nabla_x\Big) + \frac{1}{\epsilon^2}\Delta_y \tag{3.6}$$

To illustrate the homogenization procedure, we derive the Darcy's law in a perforated domain in the following Subsection.

3.2.1 Perforated domains

One limitation of the model in Paper D is the simplified geometry, as the choice of thin strip introduces a constraint in how applicable and descriptive the upscaled model can be [16]. We consider a more complex geometry with solid grains distributed periodically in the medium. Fig 3.2 shows a porous medium as a periodic perforated domain, where biofilm is attached to the grains.

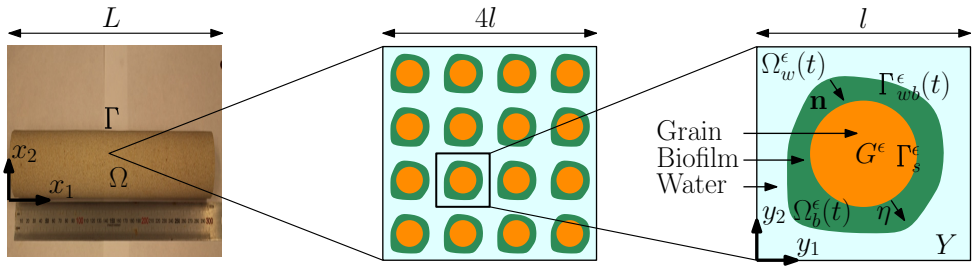

Figure 3.2: Model of a core sample with biofilm as a 2D periodic perforated domain. Photographed by Bartek Vik.

Although perforated domains are a better approximation for homogeneous porous media, we assumed that the grains are periodic. This assumption is made to derive effective quantities. The assumption on the periodicity of the porous medium allows us to simplify greatly the results, although it is not strictly necessary (and not very realistic). To have a general idea of the techniques for upscaling, we present the derivation of the Darcy's law from a pore-scale perforated domain without biofilm, where we denote by Ω_w^ϵ the water domain and Γ_s^ϵ the interface between the water and grain.

Let us denote the slow and fast variable as $\boldsymbol{x} = (x_1, x_2)$ and $\boldsymbol{y} = (y_1, y_2)$ respectively. We consider the dimensionless Stokes system:

$$\begin{cases} \epsilon^2 \mu \Delta \boldsymbol{q}^\epsilon(\boldsymbol{x}) = \nabla p^\epsilon(\boldsymbol{x}), & \text{in } \Omega_w^\epsilon, \\ \nabla \cdot \boldsymbol{q}^\epsilon(\boldsymbol{x}) = 0, & \text{in } \Omega_w^\epsilon, \\ \boldsymbol{q}^\epsilon(\boldsymbol{x}) = \boldsymbol{0}, & \text{on } \Gamma_s^\epsilon, \end{cases} \tag{3.7}$$

with initial and boundary conditions on $\partial\Omega$. The viscosity μ of order ϵ^2 physically balances the friction of the fluid on the interface. The asymptotic expansion leads to

$$\boldsymbol{q}^\epsilon(\boldsymbol{x}) = \boldsymbol{q}_0(\boldsymbol{x}, \boldsymbol{y}) + \epsilon \boldsymbol{q}_1(\boldsymbol{x}, \boldsymbol{y}) + \epsilon^2 \boldsymbol{q}_2(\boldsymbol{x}, \boldsymbol{y}) + \dots \tag{3.8}$$

$$p^\epsilon(\boldsymbol{x}) = p_0(\boldsymbol{x}, \boldsymbol{y}) + \epsilon p_1(\boldsymbol{x}, \boldsymbol{y}) + \epsilon^2 p_2(\boldsymbol{x}, \boldsymbol{y}) + \dots \tag{3.9}$$

Using the operators (3.5) and (3.6) leads to

$$\begin{cases} \mu\Delta_y \boldsymbol{q}_0 + \epsilon\mu[(\nabla_x \cdot \nabla_y + \nabla_y \cdot \nabla_x)\boldsymbol{q}_0 + \Delta_y \boldsymbol{q}_1] + O(\epsilon^2) \\ \quad = \frac{1}{\epsilon}\nabla_y p_0 + (\nabla_x p_0 + \nabla_y p_1) + \epsilon(\nabla_x p_1 + \nabla_y p_2) + O(\epsilon^2), & \text{in } \Omega_w^\epsilon, \\ 0 = \frac{1}{\epsilon}\nabla_y \cdot \boldsymbol{q}_0 + (\nabla_x \cdot \boldsymbol{q}_0 + \nabla_y \cdot \boldsymbol{q}_1) + \epsilon(\nabla_x \cdot \boldsymbol{q}_1 + \nabla_y \cdot \boldsymbol{q}_2) + O(\epsilon^2), & \text{in } \Omega_w^\epsilon, \\ \mathbf{0} = \boldsymbol{q}_0 + \epsilon \boldsymbol{q}_1 + \epsilon^2 \epsilon \boldsymbol{q}_2 + O(\epsilon^2), & \text{on } \Gamma_s^\epsilon. \end{cases} \tag{3.10}$$

Integrating $\nabla_x \cdot \boldsymbol{q}(\boldsymbol{x})$ over the water domain

$$\begin{aligned} \nabla_x \cdot \boldsymbol{q}(\boldsymbol{x}) &= \frac{1}{|\Omega_w^\epsilon|}\int_{\Omega_w^\epsilon} \nabla_x \cdot \boldsymbol{q}_0(\boldsymbol{x},\boldsymbol{y})d\boldsymbol{y} && \epsilon^0 \text{ term of } \boldsymbol{q}(\boldsymbol{x}) \\ &= -\frac{1}{|\Omega_w^\epsilon|}\int_{\Omega_w^\epsilon} \nabla_y \cdot \boldsymbol{q}_1(\boldsymbol{x},\boldsymbol{y})d\boldsymbol{y} && \nabla_x \cdot \boldsymbol{q}_0(\boldsymbol{x},\boldsymbol{y}) + \nabla_y \cdot \boldsymbol{q}_1(\boldsymbol{x},\boldsymbol{y}) = 0 \text{ from (3.10)} \\ &= -\frac{1}{|\Omega_w^\epsilon|}\int_{\partial\Omega_w^\epsilon} \boldsymbol{\nu} \cdot \boldsymbol{q}_1(\boldsymbol{x},\boldsymbol{y})d\boldsymbol{y} && \text{Gauss's theorem} \\ &= -\frac{1}{|\Omega_w^\epsilon|}\int_{\partial Y} \boldsymbol{\nu} \cdot \boldsymbol{q}_1(\boldsymbol{x},\boldsymbol{y})d\boldsymbol{y} && \text{This integral is 0 (Y-peridicity of } \boldsymbol{q}_1) \\ &\quad -\frac{1}{|\Omega_w^\epsilon|}\int_{\Gamma_s^\epsilon} \boldsymbol{\nu} \cdot \boldsymbol{q}_1(\boldsymbol{x},\boldsymbol{y})ds && \text{This integral is 0 } (\boldsymbol{q}_1 = \mathbf{0} \text{ on } \Gamma) \\ &= 0. \end{aligned}$$

This implies that the macro-scale fluid velocity is divergence free.

The ϵ^{-1} term in the first equation gives $\nabla_y p_0 = \mathbf{0}$, implying that p_0 is $y-$independent $p_0(\boldsymbol{x},\boldsymbol{y}) = p_0(\boldsymbol{x})$. The ϵ^0 terms in the first and last equation and the ϵ^{-1} term in the middle equation lead to

$$\begin{cases} \mu\Delta_y \boldsymbol{q}_0(\boldsymbol{x},\boldsymbol{y}) &= \nabla_x p_0(\boldsymbol{x}) + \nabla_y p_1(\boldsymbol{x},\boldsymbol{y}), & \text{in } \Omega_w^\epsilon, \\ \nabla_y \cdot \boldsymbol{q}_0(\boldsymbol{x},\boldsymbol{y}) &= 0, & \text{in } \Omega_w^\epsilon, \\ \boldsymbol{q}_0(\boldsymbol{x},\boldsymbol{y}) &= \mathbf{0}, & \text{on } \Gamma_s^\epsilon, \\ \boldsymbol{q}_0,\ p_1 &- Y\text{-periodic.} \end{cases} \tag{3.11}$$

We observe that

$$\nabla_x p_0(\boldsymbol{x}) = \sum_{j=1}^{2} \boldsymbol{e}_j \partial_{x_j} p_0(\boldsymbol{x}) = \boldsymbol{e}_1 \partial_{x_1} p_0(\boldsymbol{x}) + \boldsymbol{e}_2 \partial_{x_2} p_0(\boldsymbol{x}) \tag{3.12}$$

where $\boldsymbol{e}_1 = (1,0)$ and $\boldsymbol{e}_2 = (0,1)$ are the unit vectors in the x_1 and x_2 direction respectively. We assume that $\boldsymbol{q}_0$ and p_1 can be written as a linear combination of some functions $-\boldsymbol{\chi}^j(\boldsymbol{y})/\mu$ and $\Pi^j(\boldsymbol{y})$ having $\partial_{x_j} p_0(\boldsymbol{x})$ as scalars

$$\boldsymbol{q}_0(\boldsymbol{x},\boldsymbol{y}) = -\frac{1}{\mu}\sum_{j=1}^{2} \partial_{x_j} p_0(\boldsymbol{x})\boldsymbol{\chi}^j(\boldsymbol{y}), \quad p_1(\boldsymbol{x},\boldsymbol{y}) = \sum_{j=1}^{2} \partial_{x_j} p_0(\boldsymbol{x})\Pi^j(\boldsymbol{y}). \tag{3.13}$$

The choice of $-\boldsymbol{\chi}^j(\boldsymbol{y})/\mu$ allows us to identify the Darcy's law. Then, we can write (3.11) as

$$\begin{cases} -\Delta_y \boldsymbol{\chi}^j(\boldsymbol{y}) &= \boldsymbol{e}_j + \nabla_y \Pi^j(\boldsymbol{y}), & \text{in } \Omega_w^\epsilon, \\ \nabla_y \cdot \boldsymbol{\chi}^j(\boldsymbol{y}) &= 0, & \text{in } \Omega_w^\epsilon, \\ \boldsymbol{\chi}^j(\boldsymbol{y}) &= \mathbf{0}, & \text{on } \Gamma_s^\epsilon, \\ \boldsymbol{\chi}^j,\ \Pi^j &- Y\text{-periodic.} \end{cases} \tag{3.14}$$

These problems are called cell problems. To identify the solutions uniquely, we assume that $\boldsymbol{\chi}^j$ and Π^j have average 0 over Y

$$\int_Y \boldsymbol{\chi}^j(\boldsymbol{y}) d\boldsymbol{y} = \int_Y \Pi^j(\boldsymbol{y}) d\boldsymbol{y} = 0 \quad j = \{1, 2\}. \tag{3.15}$$

Defining the average as

$$\boldsymbol{q}(\boldsymbol{x}) = \frac{1}{|\Omega_w^\epsilon|} \int_{\Omega_w^\epsilon} \boldsymbol{q}_0(\boldsymbol{x}, \boldsymbol{y}) d\boldsymbol{y}, \tag{3.16}$$

we obtain the Darcy's law

$$\nabla_x \cdot \boldsymbol{q}(\boldsymbol{x}) = 0, \quad \boldsymbol{q}(\boldsymbol{x}) = -\frac{1}{\mu} \mathbb{K} \nabla p_0(\boldsymbol{x}) \quad \forall\, \boldsymbol{x} \in \Omega \tag{3.17}$$

where the components of the permeability tensor $\mathbb{K}$ are given by

$$k_{ij} = \frac{1}{|\Omega_w|} \int_{\Omega_w} \chi_i^j(\boldsymbol{y}) d\boldsymbol{y}, \quad i, j = \{1, 2\} \quad \boldsymbol{\chi}^j = (\chi_1^j, \chi_2^j) \tag{3.18}$$

For the computational point of view, the importance of this decoupling becomes obvious: instead of solving the full problem, requiring a sufficiently fine grid and thus highly complex calculations, in the upscaled case one solves much simpler problems, their number being essentially the number of nodes of a coarse grid. For this example with homogeneous viscosity and permeability, we only need to solve the two cell problems once.

3.2.2 Thin strip

Although the pore-scale model for biofilm formation of a thin strip is posed in a simplified geometry, this model is capable to capture some of the main features of the pore scale processes, and in particular of the biofilm growth in porous media. Moreover, the upscaled model, obtained in this case based on rational mathematical arguments, are in good agreement with core-scale models that are widely accepted in the literature, e.g., van Noorden et al. [100] derived an upscaled model from a pore-scale model for biofilm growth in a thin strip which is very similar to a core-scale model by Taylor and Jaffé [95]. In this manner, the upscaling provides additional support for the Taylor-Jaffé model.

Kumar et al. [53] upscaled a model in a thin strip including solute transport with mineral precipitation and dissolution. The authors found out consistency between the upscaled model and previous models for a constant geometry. We refer to Paper D for the mathematical tools for upscale the pore-scale model from Paper C in a thin strip and tube.

3.3 Effective quantities

The derived effective equations from the strip geometry describe the biofilm and nutrient concentration averaged over the width of the strip. In van Noorden et al. [100] the authors compared the upscaled model to a model proposed by Taylor and Jaffé [95]. Bringedal et al. [17] derived effective equations for mineral precipitation and dissolution in a thin strip including fluid flow and heat transport. This upscaled model are consistent with the upscaled model of [100]. In Paper D we compared the upscaled models to a model proposed by [23].

Unlike the effective parameters derived after homogenization in the thin strip, the effective parameters in perforated domains capture not only the size of the pores, but also the geometry of the pore space. However, these parameters are given by the solution of cell problems, which are challenging to solve. Bringedal et al. [18] derived effective equations for mineral precipitation and dissolution upscaling a mathematical model in a perforated domain, obtaining effective parameters of permeability and diffusion. Schulz and Knabner [89] also derived effective parameters of permeability and diffusion after upscaling a pore-scale model for biofilm growth in a perforated domain.

Hommel et al. [42] give a review of porosity-permeability relations for evolving pore space in the Darcy scale. In Paper D we compare the effective upscaled permeabilities for both geometries (thin channel and tube) using two empirical porosity-permeability relationships accounting for the biofilm permeability.

Chapter 4

Core-scale modeling

A core sample is a cylindrical piece of subsurface material. Core samples are taken from reservoirs in order to make measurements of the rock properties, such as porosity, permeability and wettability. These core samples are used to perform experiments in the laboratory. The pores in the rock can be filled with one phase (e.g. water) or several phases (e.g. water, gas and oil). Several model components, parameters and non-linearities are determined experimentally, by postulating a particular form of the equations. The role of upscaling is to derive the structure of the Darcy scale model, based on rational mathematical arguments. In previous Chapters we discussed pore-scale mathematical models for biofilms and upscaling techniques to derive core-scale effective relations and equations. The next step in our project was to use these relations to build core-scale models. In this Chapter, we describe laboratory experiments and mathematical modeling at the core scale for single- and multi-phase flow.

4.1 Single-phase flow

Henry Darcy built a mathematical model based on his experimental observations of the water flow in sand filters in 1856. This is one of the simplest mathematical models developed using laboratory experiments which is the basis of hydrogeology. Muskat improved the Darcy's law adding both fluid viscosity and density [68]. Since then, more complex laboratory experiments have been performed, leading to improved and more general mathematical models.

4.1.1 Laboratory experiments

Different experimental setups are designed to study specific processes at the core scale. Single-phase flow experiments can be used to study the permeability reduction through a core sample due to biofilm formation. In Fig. 4.1 we observe a core sample with a pressure transducer to measure changes of pressure along the core over time. As mentioned in the Introduction, biofilm formation is sensitive to environmental factors, like

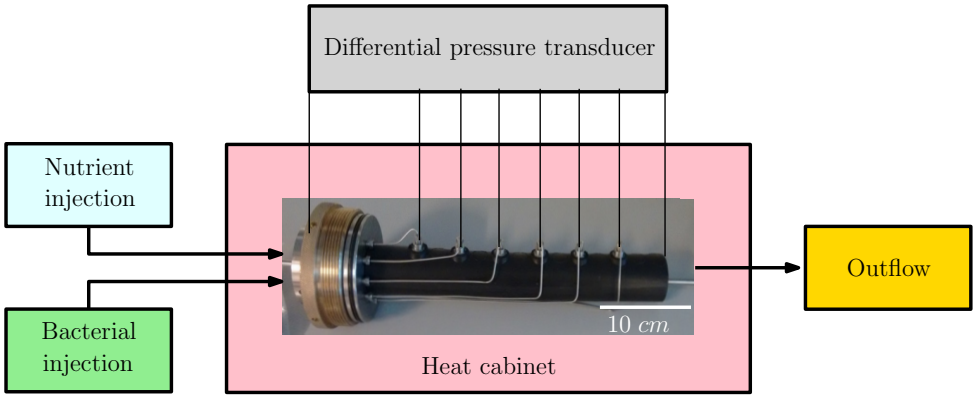

Figure 4.1: Core holder in heat cabinet for experiments. Photographed by Bartek Vik.

temperature and pH. Therefore, it is necessary to perform the experiments at the same conditions. The initial rock permeability K_0 and porosity ϕ_0 are estimated along the core before performing these experiments. After, bacteria are injected in the core-samples, which is called inoculation. The inoculation process is of the order of hours. The core is closed for some hours in order to ensure that the bacteria attach themselves to the rock. A high line pressure is held to eliminate free gases. We can distinguish two interesting study cases: measurements of changes of permeability over time at different flux injection rates and biofilm stability at different nutrient concentrations. For a given flux rate and nutrient concentration, different measurements are taken over time, such as cell counts, resistance factor and dispersion. Counting the cells in the effluent at different flow rates gives an estimate of the strength of the biofilm. The resistance factor $R_f(t)$ is given by the ratio of the pressure drop of the specific section of the clean core over the measured pressure drop of the core with biofilm. If there are no changes in the fluid rate, viscosity and density, this gives an estimate of the current rock permeability $k(t) = R_f(t)K_0$. The dispersion measurement gives an indicator of the impact of heterogeneity on the fluid flow.

Single-phase flow experiments for biofilm formation at the core-scale are also important because they allow us to study different injection techniques of nutrients to optimize biofilm growth, in the sense that we provoke the biofilm formation in a chosen part of the core using the least resources (nutrients, water, energy and time).

Another interesting single-phase flow experiment consists of studying the coupling condition on the interface between the free flow and flow in porous media [11]. For example, Palvlovskata and Meersmann [79] performed laboratory experiments using magnetic resonance imaging velocimetry methods to study the slip in velocities at the interface with a permeability discontinuity zone.

4.1.2 Mathematical modeling

On the core-scale we define the model variables on representative elementary volumes (REVs), which has a characteristic length of the order of centimeters [75]. The fluid is characterized by its density ρ (mass per unit volume) and viscosity μ (measure of fluid's resistance to flow). The porous medium is characterized by its porosity ϕ (ratio of the void volume in REV divided by the volume of REV) and permeability $\mathbb{K}$ (measure of the ease a liquid flow through the pores). In its most general form $\mathbb{K}$ is a tensor. However, for a homogeneous and isotropic porous medium can be represented as a scalar quantity.

The flux of an incompressible flow in a porous medium can be modeled using the continuity equation together with Darcy's law

$$\nabla \cdot \boldsymbol{q} = 0, \quad \boldsymbol{q} = -\frac{1}{\mu}\mathbb{K}(\nabla p - \rho \boldsymbol{g}), \tag{4.1}$$

where p is the fluid pressure and $\boldsymbol{g}$ is the gravity vector.

To model the transport of a component c in the water phase, the convection-diffusion equation is given by

$$\partial_t c + \nabla \cdot \boldsymbol{J} = 0, \quad \boldsymbol{J} = -\mathbb{D}\nabla c + \boldsymbol{q}c, \tag{4.2}$$

where in general $\mathbb{D}$ is the corresponding dispersion tensor which includes both mechanical dispersion and diffusion [10].

The bacterial formation in the rock can be modeled as

$$\frac{\partial(\rho_b \theta_b)}{\partial t} = R, \tag{4.3}$$

where θ_b is the volumetric fraction of biofilm and R is a term that accounts for the relevant processes to model, i.e., biofilm growth or bacterial detachment. The growth of bacteria will reduce the pore size in the core over time $\phi(t)$

$$\phi(t) = \phi_0 - \theta_b(t) \geq 0, \tag{4.4}$$

where ϕ_0 is the initial porosity.

As the porosity of the rock changes, we also expect that the rock permeability changes. Mathematical relations between rock permeability and porosity have been studied over the last decades [42]. One of the most common relation is given by

$$K(t) = K_0\Big(1 - \frac{\theta_b}{\phi_0}\Big)^C \tag{4.5}$$

where C is a fitting parameter.

Then, one of the simplest mathematical models for one-phase flow, nutrient transport, biofilm formation and permeability changes at the core scale is given by Eqs (4.1-4.5). This mathematical model can be extended to include more complex phenomena. For example, for a system with $n+1$ different nutrient concentrations, we can add n convection-diffusion equations (4.2). To include $m+1$ biofilm components, we can add m extra component equations (4.3).

Kim [50] built a mathematical model for bacterial transport in a saturated porous medium accounting for bacteria suspended in water, biofilm growth on the solid matrix and changes of the rock porosity due to biomass formation. The included processes for the bacteria and biofilm are reversible and irreversible biofilm attachment, detachment of biofilm, bacterial reproduction, bacterial decay and settling of bacteria due to gravity. The relation between permeability and porosity is given by Eq. 4.5 with $C = 19/6$. This mathematical model was calibrated to experimental results performed by Hendry et al. [40], who performed breakthrough experiments to study the transport and sorption of *Klebsiella oxytoka* for different sizes of silica sand columns.

4.2 Multi-phase flow

Giving that the main aim of this project is to develop a technology to enhance oil recovery, we consider multi-phase flow problems. Generally in a reservoir there is water, oil and gas. To model this system, the single-phase model equations are extended. Multi-phase flow involves distinct phases with common interfaces. Then, in the following paragraphs we introduce new concepts to model these complex systems.

4.2.1 Fundamental concepts

Let us consider a core filled with water and oil. Even if these two fluids do not mix (immiscible), they interact each other through their interfaces. We introduce new concepts to describe phenomena at these interfaces. The interfacial area (IFA) between two fluids is the common surface where both fluids are in contact. The interfacial tension (IFT) is a measurement of the excess energy present at an interface due to the imbalance of forces between molecules. Wettability is defined as the ability of a fluid phase to wet a solid surface in the presence of a second immiscible phase. For two phases, we differentiate the two phases, one wetting and the other non-wetting phase. Studying the wettability of a reservoir is important because it influences productivity and oil recovery. Capillary pressure is the pressure difference across the interface between two immiscible fluids at equilibrium, which depends upon the curvature of the interface separating the fluids. To account for flow interactions between multiple phases, we introduce the concept of relative permeabilities, which account for reduction of flow compared to when the pores are only saturated by one phase. The relative permeabilities depend on the fluid properties and flow mechanisms.

Hysteresis is the dependence of the state of a system on its history. Let us consider a core saturated with water. The displacement of a non-wetting phase by a wetting phase in porous media is called imbibition, while drainage is the reverse process. Early experiments to measure capillary pressures and relative permeabilities after drainage and imbibition showed the presence of hysteresis. This hysteresis is attributed to different fluid-fluid behavior if the flux reverses.

Once we have introduced new definitions for multi-phase flow, in the next Subsections we give a general description of multi-phase flow laboratory experiments and math-

ematical modeling techniques.

4.2.2 Laboratory experiments

In Section 4.1 we describe single-phase flow laboratory experiments. The importance of these experiments for the bio-plug technology relies on studying biofilm properties such as strength, composition and maturity. The next step is to test the bacteria in presence of oil at real reservoir conditions, such as pH, temperature and salinity. Core samples from oil fields or outcrop may be used to perform experiments at reservoir conditions.

To study the bio-plug technology in the presence of oil and water one possibility is to consider several cores with similar rock properties but at different initial oil saturations. Then, different inoculation strategies and nutrient injections can be tested in order to study the oil recovery. As mentioned before, for strategies of injection one can modify the nutrient concentration, the flow rate and the flow direction.

As mentioned in the Introduction, some biofilms produce gases. When the biofilm is surrounded by water and oil, these gases might dissolve in the fluid phases or be present as an extra phase. When an extra phase appears in the system this increases the complexity of performing experiments because it is more challenging to control, measure and characterize the additional physical, biological and chemical processes in the system. Then, one strategy to eliminate the produced gasses is to apply a line pressure to the system.

Suthar et al. [94] performed laboratory experiments in core samples using *Bacillus licheniformis TT33* to study the selective plugging strategy for MEOR. This organism produces both EPS and surfactants. After brine flooding, around 50% of oil remained unrecovered. The *Bacillus licheniformis TT33* allowed them to recover around 25% of additional oil. Then, the authors concluded that this organism has a potential for field applications.

Fujiwara et al. [34] presented a study to show the effectiveness of MEOR in reservoirs based on the results of laboratory experiments and MEOR field tests. The studied MEOR strategy was selective plugging. First, core samples from the reservoir were taken to identify microbes inhabiting the reservoir rock. A strain CJF-002, belonging to the genus *Enterobacter*, were selected as the microbes. Before field tests, experiments in core-samples were performed in the laboratory to asses the permeability reduction. The experiments confirmed that these microbes have the ability to modify core permeabilities. Two field trials were performed to study the increase of oil production using the strain CJF-002. They observed a dramatic increase in oil production 20 days after beginning injections. Even after stopping the injection of bacteria and nutrients, the oil recovery rate after one year was still doubled. The authors also present a cost-benefit analysis, concluding that MEOR increases oil recovery in an economically attractive manner.

4.2.3 Mathematical modeling

To model multi-phase immiscible flow, we can introduce the saturation of a phase α as the ratio of the phase volume in REV divided by the void volume in REV, denoted by s_α. This implies that for n phases $\sum_\alpha^n s_\alpha = 1$. To model the flow of each phase, we can use the mass conservation and the extended multi-phase Darcy's law

$$\frac{\partial}{\partial t}(\rho_\alpha s_\alpha \phi) + \nabla \cdot (\rho_\alpha \boldsymbol{q}_\alpha) = 0, \quad \boldsymbol{q}_\alpha = -\frac{1}{\mu_\alpha}\mathbb{K}k_{r,\alpha}(\nabla p_\alpha - \rho_\alpha \boldsymbol{g}), \tag{4.6}$$

where $k_{r,\alpha}$ is the relative permeability of phase α. The relative permeabilities take values between 0 and 1. To relate two phase pressures p_w and p_n, the capillary pressure p_{nw} is used

$$p_n - p_w = p_{nw}. \tag{4.7}$$

Empirical correlations of relative permeability and capillary pressure are often used. These relations are given as a function of the phase saturation and diverse fitting parameters. The Brook-Corey relations are commonly used to model the relative permeability relations and capillary pressure. For a two-phase flow problem $\alpha = \{w, n\}$, these relations are given by

$$p_c(s_w^*) = p_e s_w^{*-1/\lambda}, \quad k_{r,w}(s_w^*) = k_{rwnr} s_w^{*\alpha}, \qquad k_{r,n}(s_n^*) = k_{rnwr} s_n^{*\beta}, \tag{4.8}$$

where p_e is the entry pressure, λ, α and β are fitting parameters, k_{rnwr} is the endpoint relative permeability of the phase n and k_{rwnr} is the endpoint relative permeability of the phase w. The effective saturations s_w^* and s_n^* are given by

$$s_w^* = \frac{s_w - s_{wr}}{1 - s_{nr} - s_{wr}}, \quad s_n^* = \frac{s_n - s_{nr}}{1 - s_{nr} - s_{wr}}, \tag{4.9}$$

where s_{wr} and s_{nr} are residual saturations of each phase respectively.

For describing the fluxes of two immiscible fluids n and w, we have six equations and unknowns s_n, p_n, q_n, s_w, p_w and q_w.For the interested reader we refer to the work of Holm [41] for modeling of three-phase flow for MEOR.

We mentioned before that hysteresis is presented in the capillary pressure and relative permeabilities. One strategy to capture this process is to modify the fitting parameters to obtain different curves for drainage and imbibition. Another option to model hysteresis is to include one extra equation to model the interfacial area a_{wn}. Then, the capillary pressure curve can be extended to a surface and estimated from experiments as a function of saturation and interfacial area $p_{nw}(s_n, a_{wn})$.

The residual oil saturation s_{or} is the oil that remains in a porous media after water injection. To model the effects of water and surfactant for recovering the s_{or}, we introduce the concept of capillary number N_C. The capillary number is the main factor affecting displacement efficiency, which relates surface tension and viscous forces action on the oil-water interface and is given by

$$N_C = \frac{q_w \mu_w}{\sigma_{nw}} \tag{4.10}$$

where σ_{nw} is the oil-water interfacial tension. From Eq. (4.10) we observe that increasing the water flux, water viscosity or decreasing the interfacial tension would lead to an increase in the capillary number. We previously mentioned that one mechanism for MEOR is to use the produced surfactants c_s to lower the interfacial tension between oil and water. In the literature, there exists different experimentally calibrated relationships between the surfactant concentration and interfacial tension $\sigma_{nm}(c_s)$. Laboratory experiments and fitting functions of residual oil saturation and capillary number $s_{or}(N_C)$ are used to model the increase of oil recovery using different MEOR effects [38].

Nielsen et al. [73] built a core-scale mathematical model for two-phase flow including transport of nutrients and bacteria in the water phase, bacterial growth, bacterial attachment, detachment, sporulation, nutrient consumption, surfactant production and residual oil saturation reduction due to surfactants. This mathematical model can be applied to study injection techniques for optimizing the MEOR process.

In Paper E we present the model equations for a core filled with water and oil including permeability changes due to biofilm growing. In Paper F we proposed a novel mathematical model for a core filled with water and oil including the interfacial area between the oil and water, hysteresis, transport of nutrients and bacteria, production of surfactants and interfacial tension reduction.

Chapter 5

Numerical framework

Mathematical models for MEOR are based on coupled nonlinear partial differential equations (PDEs) and ordinary differential equations (ODEs), which may be very difficult to solve. The challenging aspects in the numerical solution of pore-scale models are due to the coupling of the non-linearities and the existence of free boundaries (the biofilm-water interface) as it needs to be determined as part of the solution process. Therefore, it is necessary to use advanced numerical methods and simulations to predict the transient behavior of model variables in these complex systems.

5.1 Space discretization

Discretization is the process of representing a continuum with a finite set of elements. To solve numerically the mathematical equations describing a system in a domain, it is necessary to divide the domain into a collection of finite elements. This allows us to approximate the flow equations by algebraic equations that can be solved in each element. In this work we used two space discretization methods: finite volume and finite element. In reservoir simulation, it is possible to combine both methods to solve the system of equations [107].

5.1.1 Finite volume methods

The presentation of this Section is based on [59]. The finite-volume discretization used in this work was the two-point flux-approximation (TPFA) scheme. One of the advantages of using finite volume methods is that are intrinsically conservative. To show how to apply this method, we consider the single-phase flow equation in a 2D Cartesian grid $\Omega \subset \Re^2$ with isotropic permeability

$$\nabla \cdot \boldsymbol{v} = q, \quad \boldsymbol{v} = -K\nabla p. \tag{5.1}$$

Fig. 5.2 shows two cells in a 2D Cartesian grid with dimensions, pressures, permeabilities, interface and flux across the interface. We integrate the previous equation in the

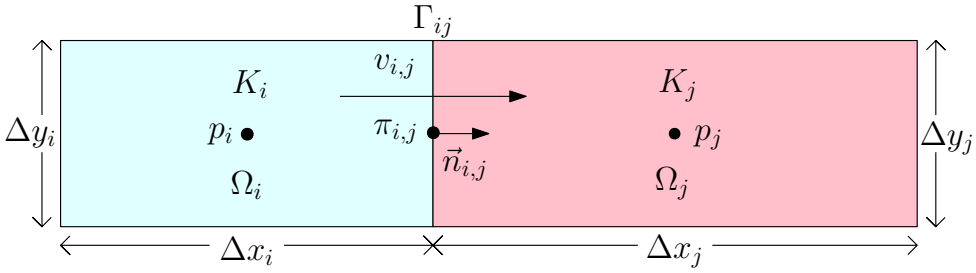

Figure 5.1: Cells Ω_i and Ω_j in a Cartesian grid to derive the TPFA discretization (adapted from [59]).

control volume Ω_i

$$\int_{\Omega_i} \nabla \cdot \boldsymbol{v} d\boldsymbol{x} = \int_{\partial\Omega_i} \boldsymbol{v} \cdot \boldsymbol{n} ds = \int_{\Omega_i} q d\boldsymbol{x}, \tag{5.2}$$

where we have used the Gauss's theorem. Next, we focus on the flux across each face of the cell Γ_{ij} ($\Gamma_{ij} = \partial\Omega_i \cap \partial\Omega_j$)

$$v_{i,j} = \int_{\Gamma_{ij}} \boldsymbol{v} \cdot \boldsymbol{n} ds. \tag{5.3}$$

Assuming that the integral over Γ_{ij} is approximated by the midpoint rule, then using the Darcy's law we can write (5.3) as

$$v_{i,j} \approx -A_{i,j}(K\nabla p)(\boldsymbol{x}_{i,j}) \cdot \boldsymbol{n}_{i,j}, \tag{5.4}$$

where $A_{i,j}$ is the length of the interface Γ_{ij}, $\boldsymbol{n}_{i,j}$ is the unitary normal vector and $\boldsymbol{x}_{i,j}$ denotes the geometric center of Γ_{ij}. Next, we assume that the average value of pressure is constant inside each cell, resulting in

$$v_{i,j} = \Delta y K_i \frac{p_i - \pi_{i,j}}{(\frac{1}{2}\Delta x_j)^2}(-\tfrac{1}{2}\Delta x_i, 0)(1,0)^T = \Delta y \frac{2K_i}{\Delta x_i}(p_i - \pi_{i,j}), \quad v_{j,i} = \Delta y \frac{2K_j}{\Delta x_j}(p_j - \pi_{j,i}),$$

where we have define $\Delta y := \Delta y_i = \Delta y_j$. Assuming continuity of fluxes ($v_{i,j} = -v_{j,i} := v_{ij}$) and face pressures ($\pi_{i,j} = \pi_{j,i} := \pi_{ij}$) across the cells, we can eliminate π_{ij} to obtain

$$v_{ij} = 2\Delta y \Big(\frac{\Delta x_i}{K_i} + \frac{\Delta x_j}{K_j} \Big)^{-1} (p_i - p_j).$$

We observe that the permeability on the interface is approximated by the harmonic mean. Then, the TPFA scheme leads to a symmetric system of equations which solution is defined up to an arbitrary constant. In MRST, this is done by choosing $p_1 = 0$. Let us consider now the steady transport equation

$$\nabla \cdot (c\boldsymbol{v}) = R(c) \tag{5.5}$$

where $\boldsymbol{v}$ is the water velocity and c the concentration of a solute in the water. Analogously to the single-phase flow equation, if we can define an appropriate value c_{ij} at the interface Γ_{ij}, we can write the flux across the interface as

$$\int_{\Gamma_{ij}} c\boldsymbol{v} \cdot \boldsymbol{n} ds = c_{ij} v_{ij}. \tag{5.6}$$

The upstream weighting is used to give the value of the concentrations at the interface Γ_{ij}

$$c_{ij} = \begin{cases} c_i, & \text{if } v_{ij} \geq 0, \\ c_j & \text{otherwise.} \end{cases} \tag{5.7}$$

TPFA methods fail to converge if the grid directions are not aligned with the principal directions of the permeability tensor K. For problems involving heterogeneous media and irregular grid structures, multi-point flux approximation (MPFA) methods can be used to solve the model equations [1, 86]. The core-scale model in Paper E was implemented in the MATLAB® reservoir simulation toolbox (MRST) [59] and the core-scale mathematical model in Paper F was implemented in MATLAB® , in both implementations the TPFA scheme was used.

5.1.2 Finite element methods

This entire Subsection is primarily based on [47]. To show how to apply this method, we consider the Poisson equation in a 2D bounded open domain $\Omega \subset \Re^2$

$$-\Delta c = f \text{ in } \Omega, \quad c = 0 \text{ on } \Gamma, \tag{5.8}$$

where Γ is a polygonal curve and f is a given function. Let $v \in V$ be a function such that $V = \{v : v \text{ is continuous on } \Omega, \ \partial v/\partial x_1 \text{ and } \partial v/\partial x_2 \text{ are piecewise continuous on } \Omega \text{ and } v = 0 \text{ on } \Gamma\}$. Then, multiplying (5.8a) by v, applying the divergence theorem and using the boundary condition of v on Γ lead to

$$-\int_\Omega v\Delta c d\boldsymbol{x} = \int_\Omega \nabla v \cdot \nabla c d\boldsymbol{x} - \cancelto{0}{\int_\Gamma v \frac{\partial c}{\partial n} ds} = \int_\Omega v f d\boldsymbol{x} \tag{5.9}$$

Then, we can formulate the following variational problem: Find $c \in V$ such that $a(u, v) = l(v)\ \forall v \in V$, where

$$a(u, v) = \int_\Omega \nabla c \cdot \nabla v d\boldsymbol{x}, \quad l(v) = \int_\Omega f v d\boldsymbol{x}. \tag{5.10}$$

It is possible to show that if c satisfies (5.8), then c is the solution of the previous variational problem and vice versa. Now, we make a triangulation of Ω

$$\Omega = \bigcup_{K \in T_h} K \tag{5.11}$$

where no vertex of one triangle lies on the edge of another triangle. Then, we can con-

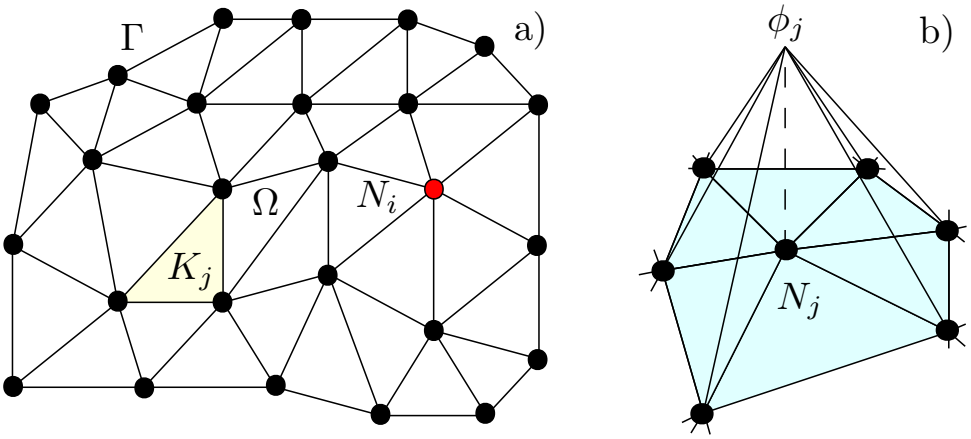

Figure 5.2: A finite element triangulation a) and the basis function b) (adapted from [47]).

struct the following finite-dimensional subspace of V: $V_h = \{v : v \text{ is continuous on } \Omega, v|_K \text{ is linear for } K \in T_h,\ v = 0 \text{ on } \Gamma\}$, where $v|_K$ denotes the restriction of v to K. Excluding the nodes on the boundary ($c = 0$ on Γ), let M be the number of nodes in Ω. Then, defining the following basis functions:

$$\phi_j(N_i) = \begin{cases} 1 & \text{if } i = j, \\ 0 & \text{otherwise,} \end{cases} \tag{5.12}$$

a function $v \in V_h$ evaluated in $\boldsymbol{x} \in \Omega \cup \Gamma$ can be written as $v(\boldsymbol{x}) = \sum_{j=1}^{M} \eta_j \phi_j(\boldsymbol{x})$, where $\eta_j = v(N_j)$. Then, we can formulate the following finite element method: Find $c_h \in V_h$ such that $a(c_h, v) = (f, v)\ \forall v \in V_h$. This is equivalent to a linear system of equations $A\boldsymbol{y} = \boldsymbol{b}$ where A is called stiffness matrix and it is a $M \times M$ matrix with elements $a_{ij} = a(\phi_i.\phi_j)$ and $\boldsymbol{y}$ and $\boldsymbol{b}$ are vectors of size M with elements given by $y_i = c_h(N_i)$ and $b_i = (f, \Phi_i)$.

The mathematical models in Papers A, C and D were implemented in the commercial finite element software COMSOL Multiphysics® software [25].

5.2 Free boundary problems

Free boundary problems appear among other cases in the following areas [32]: melting and solidification phenomena (Stefan problems), obstacle problems for elastic membranes, contact problems with elastic deformation, growth of tumors, flows with free surfaces and the modeling of financial derivative products. The interface tracking methods include: level set method, phase field method and arbitrary Lagrangian-Eulerian method ALE.

5.2.1 Phase field method

The phase field method was introduced by Fix [33] and Langer [58] in the 1980s. A phase-field model describes a microstructure, both the structural domains and the interfaces, as a whole by using a set of field variables which are continuous across the interfacial regions and hence the interfaces in a phase-field model are diffused [63]. The phase field interface also allows us to model fluid-structure interaction and phase separations. The phase field method has been applied for different mathematical models, e.g., crack propagation in a poroelastic medium [65] and ion precipitation in a porous media [85]. It has been extensively used for modeling biofilm systems [60, 96, 110].

5.2.2 Level set method

While the phase field method is based on physical considerations, the level set method has been developed from a mathematical point of view and corresponds to a color function that is convected by the fluid flow. The level set method was introduced by Osher and Sethian [77] in 1988. The level set method represents an interface Γ as the zero-contour of a higher dimensional function denoted by Φ

$$\Phi(\boldsymbol{x}) = \begin{cases} -d, & \text{for } \boldsymbol{x} \in \Omega^-, \\ d, & \text{for } \boldsymbol{x} \in \Omega^+, \\ 0, & \text{for } \boldsymbol{x} \in \Gamma, \end{cases}$$

where d is the Euclidian distance to Γ. The interface deforms according to the level-set equation under a velocity field $\boldsymbol{v}$ as

$$\partial_t \Phi + v_n |\nabla \Phi| = 0, \quad \text{where } v_n = \boldsymbol{v} \cdot \boldsymbol{n} \text{ and } \boldsymbol{n} = \nabla\Phi/|\nabla\Phi|.$$

We refer to [36] for a review of level set methods.

5.2.3 ALE method

The following presentation of the ALE method is based on the work by Donea et al. [28]. To model the kinematics of a particle through space and time, two descriptions are usually used: Lagrangian and Eulerian approaches. Normally, the Lagrangian description is used in solid mechanics and the Eulerian description is used in fluid mechanics. Let us consider a one-dimensional domain with four particles as shown in Fig. 5.3. Initially, the mesh nodes and the material points overlap. In Lagrangian algorithms, each node of the mesh follows the corresponding material particle during motion. One of the disadvantages of this description is that the mesh can suffer large distortions because the mesh deforms with the material. In Eulerian algorithms, the mesh is fixed. However, it is difficult to set boundary and interface conditions. The arbitrary Lagrangian Eulerian (ALE) description aims to combine the best features of these two descriptions. The ALE algorithm allows us to track the moving interfaces and boundaries. Let us denote by (R_x, x) and (R_X, X) the reference configurations and coordinates for the Eulerian

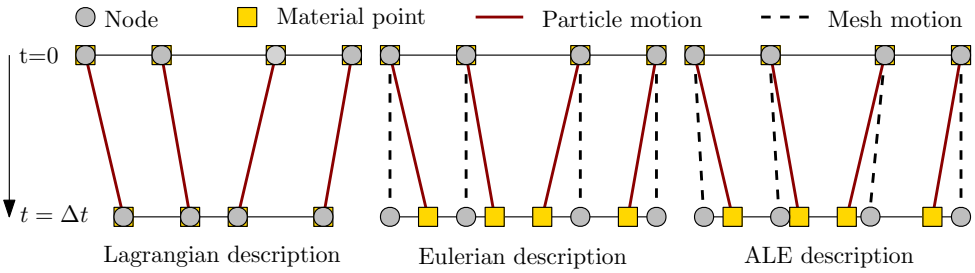

Figure 5.3: Example of mesh and particles displacement in the three different descriptions (adapted from [28]).

and Lagrangian descriptions respectively. To write the mathematical equations from the ALE point of view, it is necessary to consider a new spatial configuration R_χ and reference coordinates χ. Let us denote by $\boldsymbol{v}$ the mesh velocity $\boldsymbol{v} = \partial \boldsymbol{x}/\partial t|_{\boldsymbol{\chi}}$, where $|_{\boldsymbol{\chi}}$ means that the material coordinate $\boldsymbol{\chi}$ is kept fixed. Then, the mass conservation in the three different descriptions is written as

$$\text{Eulerian description} \qquad \left.\frac{\partial \rho}{\partial t}\right|_x + \nabla \cdot (\rho \boldsymbol{q}) = 0 \tag{5.13}$$

$$\text{Lagrangian description} \qquad \left.\frac{\partial \rho}{\partial t}\right|_X + \rho \nabla \cdot \boldsymbol{q} = 0 \tag{5.14}$$

$$\text{ALE description} \qquad \left.\frac{\partial \rho}{\partial t}\right|_\chi + \rho \nabla \cdot \boldsymbol{q} + \boldsymbol{c} \cdot \nabla \rho = 0 \tag{5.15}$$

where $\boldsymbol{c} = \boldsymbol{q} - \boldsymbol{v}$ is the relative velocity between the material and the mesh. For the mass conservation in the ALE description, we observe that when the mesh velocity is zero, the equation corresponds to the Eulerian description and when the mesh velocity is equal to the material velocity, the equation is written as in the Lagrangian description.

In principle, one can decide the mesh-update procedure which assigns the mesh-node velocities or displacements at each time step. There are two common strategies: mesh regularization and mesh adaption. The interested reader may find a description of mesh-update procedures in [28]. The main drawback of the ALE method is the fact that the mesh must deform continuously, which means that problems involving topological changes cannot be solved. Fortunately, in our case, these deformations remain smooth and therefore, we choose this method to solve the governing equations.

5.3 Time discretization

We have given discretization techniques for the spatial differential operators which do not depend on time. As in the spatial domain, it is necessary to discretize the temporal domain to find a numerical solution. Let us consider the following partial differential equation

$$\frac{\partial}{\partial t}\boldsymbol{u}(\boldsymbol{x}, t) = F(\boldsymbol{u}, \boldsymbol{x}, t). \tag{5.16}$$

Then, using the first-order derivative discretization, we can write the previous equations as

$$\frac{\boldsymbol{u}(\boldsymbol{x}, t+\Delta t)-\boldsymbol{u}(\boldsymbol{x}, t)}{\Delta t} \approx F(\boldsymbol{u}, \boldsymbol{x}, t). \tag{5.17}$$

The approximation of the function F leads to different time discretization methods. One of the explicit methods consist of evaluating the function F in the time t, resulting in

$$\boldsymbol{u}^{n+1} = \boldsymbol{u}^n + F^n \Delta t \tag{5.18}$$

where $\boldsymbol{u}^{n+1} = \boldsymbol{u}(\boldsymbol{x}, t+\Delta t)$, $\boldsymbol{u}^n = \boldsymbol{u}(\boldsymbol{x}, t)$ and $F^n = (\boldsymbol{u}, \boldsymbol{x}, t)$. This time discretization is known as forward Euler method. One of the most used implicit time discretization methods is the backward Euler method, given by

$$\boldsymbol{u}^{n+1} = \boldsymbol{u}^n + F^{n+1} \Delta t. \tag{5.19}$$

More general explicit and implicit time discretizations are given by the Runge-Kutta methods. In Papers A, C, D, E and F, the backward Euler method is used for the time discretization.

5.4 Numerical solvers

After discretizing in space and time the model equations, iterative schemes can be used to solve systems of non-linear coupled equations. Linearization schemes such as Newton's method, Picard's method, the Picard/Newton's method or the L-scheme [61, 78, 84] are used to solve numerically flow and reactive transport models.

Let us consider the following non-linear vector equation

$$F(\boldsymbol{x}) = \boldsymbol{0} \quad (F : X \to Y), \tag{5.20}$$

where X and Y are Banach spaces. The Newton's method (also known as Newton-Rapshon's method) has the form $x_{k+1} = x_k - [F'(x_k)]^{-1} F(x_k)$, where F' is the Fréchet derivative of F [35]. The Newton-like methods are defined by

$$x_{k+1} = x_k - [M(x_k)]^{-1} F(x_k), \tag{5.21}$$

where $M(x)$ is usually an approximation to $F'(x^*)$, where x^* is a solution of (5.20). For example, a common variant of these methods is the damped Newton method: $x_{k+1} = x_k - t_k [F'(x_k)]^{-1} F(x_k)$, where $t_k > 0$ it is the damping factor. The Newton-Rapshon's method has a quadratic order of convergence. However, it requires that the initial guess is close enough to the solution, which restrict the time step and it also requieres that the derivative F' is known, which may be difficult to compute. In MRST, automatic differentiation is used to compute this derivative [52].

5.5 Parameter estimation

As mentioned in the Introduction, measurements of the input parameters for the mathematical models need to be improved. Aksoy [3] defines parameter estimation as the determination of the best values of specific parameters in a mathematical model through data assimilation or other similar techniques. Aksoy comments on two main purposes of parameter estimation: first, detailed and targeted observations and advanced data assimilation techniques can be used to gain a better understanding of the parameterized physical processes themselves and second, to improve the model state with the parameters to be estimated, i.e., improve numerical forecasts acknowledging uncertainties in initial conditions and the model.

Let us consider the Monod's equation $\mu(c) = \mu_{max} c/(k_n + c)$ to model the biofilm growth, where μ_{max} is the maximum specific growth rate and k_n is the half-saturation concentration. To give better estimates of these coefficients for different organism is an active research field. Both coefficients μ_{max} and k_n can be estimated by various linearization methods such as the Hanes-Woolf plot, the Eadie-Hofstee diagram and the Lineweaver-Burk plot [92]. The Hanes-Woolf plot consists on rearranging the terms in the Monod's equations as

$$\frac{c}{\mu(c)} = \frac{c}{\mu_{max}} + \frac{k_n}{\mu_{max}}. \tag{5.22}$$

Then, the slope of the line corresponds to $1/\mu_{max}$ and the interception with the c-axis to $-k_n$. More accurate estimations of these parameters are done using nonlinear regression methods [37].

In Paper C, we estimate the value of the stress coefficient k_{str} for the bacterium *Thalassospira* strain A213101, using the measurements of biofilm coverage area over time for four different flux velocities. To better estimate the value of this parameter, it is necessary to repeat the experiments for more different flux velocities and to have better estimates of the remaining model parameters and initial conditions.

5.6 Sensitivity analysis

Due to the cost of performing laboratory experiments to accurately estimate material parameter values, it is of great interest to perform a sensitivity study with respect to the impact of a set of input parameters on certain model output quantities of interest. A parametric analysis or sensitivity analysis is the study of the influence of different geometric or physical parameters or both on the solution of the problem.

The simplest method to sensitivity analysis is to repeatedly vary one parameter at a time while holding the other fixed which is known as one-at-a-time sensitivity measures [39]. In Paper A we performed an one-at-a-time sensitivity measures for some input parameters such as nutrient concentration, entry pressure and biofilm permeability. The plots show different biofilm height profiles for different values of the parameters. Studying one parameter at the time allows us to identify the value of the parameter that produces a given output, i.e., we could identify the minimum nutrient concentration which

produces the maximum biofilm growth in a given time. However, this simple sensitivity analysis cannot identify interactions between input variables.

Global sensitivity analysis using Sobol indices is a means of quantifying the relative impact of a function of interest in terms of a set of varying input parameters [93]. This sensitivity analysis ensures the identification of critical parameters. Moreover, for parameters scoring low in sensitivity estimates, less accurate parameter estimates can be justified. In the Appendix A of Paper C, the theory behind this global sensitivity analysis is described.

Chapter 6

Summary, conclusion and outlook

In this chapter, we summarize the scientific results presented in the form of six scientific articles in Part II. Paper A presents a pore-scale mathematical model for biofilm formation based on previous scientific works. A detailed description of the performed laboratory experiments in a micro-channel is given in Paper B. A modified pore-scale model is built in Paper C based on the findings in Paper B. Paper D presents in detailed the upscaling of this pore-scale model for two different different geometries and compares the derived effective quantities. In Paper E we describe the conducted laboratory experiments at the core-scale and built a two-phase flow mathematical model for the bio-plug technology. A novel two-phase flow model for microbial enhanced oil recovery including the oil-water interfacial area is discussed in paper F. The conclusion and outlook finalize the Part I of this dissertation.

6.1 Summary of the papers

Paper A: *Numerical simulation of biofilm formation in a microchannel*

Biofilms are formed by different components, such as water, bacteria and polymers. Therefore, it is important to include the effects of water and different components in the development of biofilms. van Noorden et al. [100] upscaled a pore-scale model including biofilm growth, erosion, attachment, bacterial decay and transport of nutrients and bacteria by advection and diffusion in a thin channel. Alpkvist and Klapper [4] built a mathematical model for a heterogeneous biofilm. Inspired by these models, we developed a mathematical model for biofilm formation in a thin strip which includes biofilm components (water, bacteria, EPS and dead bacteria), permeability and porosity.

The biofilm is assumed to grow symmetrically in the upper and lower walls. The flow in the water phase is modeled using the mass conservation and Stokes equation, while the flow inside the biofilm by the mass conservation and Darcy's law. The nutrients are transport in the water phase and inside the biofilm by advection and diffusion. Conservation of mass is imposed for each of the biomass components. To model the movement of biomass due to bacterial reproduction, production of EPS and death of bacteria, a growth

potential is assumed. Then, the biomass velocity is given by the gradient of the growth potential. The mathematical model involves a moving interface between the biofilm and water. Then, coupling conditions are needed on the interface. To couple the water fluxes, we consider the water mass balance, the equilibrium of normal forces and the Beavers-Joseph-Saffman condition on the interface. The nutrients are assumed continuous across the interface and in addition we consider the Rankine-Hugoniot condition to describe the speed of this interface.

To solve numerically this coupled system of non-linear partial differential equations, it is necessary to use advance numerical methods. Linear Garlekin finite element were used for the spatial discretization, while backward Euler for the time discretization. A damped version of Newton's method is used in each of the temporal steps. The movement of the oil-water interface was updated using an arbitrary Lagrangian-Eulerian (ALE) method. The iterative scheme is the following: first we solve for the pressures and water fluxes, secondly we solve for the nutrient concentrations, thirdly we solve for the volume fractions, growth potential and biofilm thickness; after we iterate between the three previous steps until the difference between successive values of the solution drops below a given tolerance and thereafter we move to the next time step and repeat the process until the given final time.

A parametric study (one at-a-time) is performed to study the influence of the nutrient concentration, pressure and biofilm permeability on the biofilm profile over time. The results show changes in the biofilm height when these three parameters increase or decrease in one or two orders of magnitude. As expected, the biofilm height increased when we increase either the nutrient concentration or biofilm permeability and decreased when we increase the input pressure.

One of the outcomes from the numerical simulations is that the flux inside the biofilm can be neglected for low flow rates. However, for higher flow rates we must consider the effects of the water flow inside the biofilm, that affects the transport of nutrients and the flux velocity value at the interface which changes the biofilm thickness via the stress force.

One of the aims of this first paper was to solve the highly coupled set of equations using numerical techniques. The next step was to modify and calibrate the pore-scale model with the experiments described in Paper B.

Paper B: *Microfluidic study of effects of flow velocity and nutrient concentration on biofilm accumulation and adhesive strength in the flowing and no-flowing microchannels*

The bacteria *Thalassospira* strain A216101, a facultative anaerobic, nitrate-reducing bacteria, capable of growing under both aerobic and anaerobic conditions, was used in this work. Bacteria were enriched in a marine mineral medium referred as growth medium. Pyruvate was added as the carbon source to achieve final nutrient concentrations of 1 mM (millimolar), 5 mM, 10 mM and 20 mM. To avoid biofilm clogging at the inlet channel, a microchannel with two inlets and one outlet is used. We refer to the

inoculation channel as channel two, while the channel where nutrients are injected and the effluent flow is refer as channel one. A T-shape microchannel with sizes of 100 μm width, 20 μm depth and the nuzzle size at the cross-section roundly 10 μm. The experiments were performed at room temperature and atmospheric pressure. To aim for similar initial biofilm attachment conditions, the microchanel was cleaned before every inoculation. The following sentences explain the inoculation process. First, the bacteria were pre-cultured in a growth medium with 10 mM at 30 °C for 24 hours. The left channel was closed and the pre-culture bacterial solution was injected through the lower channel at a rate of 1.0 μ l/min for 24 hours. After, the whole system was closed for 24 hours.

Different experiments at different fluid injection rates and nutrient concentrations were performed to study the percentage of biofilm coverage in two different sections in the microchannel. The flow rates were 0.2 μ l/min, 0.3 μ l/min, 0.4 μ l/min and 0.5 μ l/min, which correspond to a water velocity of 1.66 mm/s, 2.50 mm/s, 3.33 mm/s and 4.17 mm/s respectively. The nutrient concentration of 10mM is taken as a reference concentration, denoted as 1.0 N.

A leica microscope together with a digital camera were used to capture the biofilm development over time. The different intensity in pixels on the images were used to estimate the biofilm growth using the MATLAB Image Processing Toolbox. A quantitative polymerase chain reaction (qPCR) was performed to estimate the total number of bacteria in the effluent. The total number of bacteria revealed that for nutrient concentration of 1 N and 0.5 N are sufficient for biofilm growth, contrary to the low concentration of 0.1 N.

The experimental results show that both nutrient concentration and flow velocity control biofilm development in the microchannel. At the rate flow of 0.2 μ l/min (1.66 mm/s) and nutrient concentration of 1.0 N (10 mM), a strong plugging in the microchannel was observed to resist higher shear forces due to increase in the flux rate.

These experimental results and observations contributed to the formulation and calibration of the pore-scale model presented in Paper C.

Paper C: *A pore-scale model for permeable biofilm: numerical simulations and laboratory experiments*

The aim of this paper is the calibration of a pore-scale mathematical model for biofilm formation in a thin channel. The developed mathematical model includes relevant processes observed in the experiments. In Paper A we introduce the mathematical model. In this Paper we assume that the biofilm grows only in the lower wall, in contrast to the symmetry assumption in Paper A. The reason for this is that the experiments in Paper B were performed in a T-channel, then after inoculation the biofilm started to form in the lower channel. Moreover, based on that biofilms are mostly formed by water [2], we consider the Brinkman equation instead of Darcy's law to model the flow inside the biofilm. The reason for this is that the Brinkman model is derived from the Stokes model assuming that the volume of the porous media skeleton is much smaller than the volume of the reference cell, which is the case for most biofilms.

To calibrate the mathematical model, we used input data from the experiments performed in Paper B. Using parameters from the literature, we aimed to calibrate the stress coefficient. Then, we considered measurements of biofilm coverage area over time for four different flux rates. The nutrient concentration was kept constant. We found a stress coefficient of the order or $10^{-}10$ m/(s Pa) which captured best the decrease of the coverage area as the flux rate increased.

In Paper A a simple parametric study was performed to study the variability of the biofilm height when input parameters such as boundary condition for the pressure, inlet nutrient concentration, and the parameter describing the biofilm permeability were changed. For a more complete study of the variability in input parameters on the numerical results, we performed a sensitivity study. Then, a global sensitivity analysis [93] was performed to quantify the effect of variability or uncertainty in ten material parameters on the biofilm coverage area. The analysis showed that the maximum growth rate is the most critical parameter, but all ten parameters should be estimated with sufficient accuracy to improve the reliability of the biofilm coverage area.

The next step in the project was to upscaled this pore-scale model in different pore geometries to derive core-scale models, which is treated in Paper D.

Paper D: *An upscaled model for permeable biofilm in a thin channel and tube*

This paper shows the details for upscaling the pore-scale model developed in Papers A and C based on the experiments in Paper B. The homogenization techniques followed in this paper were inspired by the work of van Noorden et al. [100]. In that work the authors upscaled a pore-scale model for impermeable single-component biofilm in a thin channel. The novelty of our work is the upscaling of a pore-scale permeable multi-component biofilm in a thin channel and tube. One of the motivations for choosing these geometries is that experiments are performed in different pore geometries (e.g. microchannels and tubes) and some porous media can be modeled as a stack of these pore geometries.

The pore-scale model in Papers A and C is built in a thin channel geometry. In the Appendix of this Paper we show the technicalities to upscale the model in a thin channel. In the main body of this Paper, the equations are described in a tubular geometry. We define the new domain using cylindrical coordinates. We assume radial symmetry for the biofilm growth. Initially, biofilm is attached to the pore walls. Water and nutrients are injected into the pore. The mathematical model includes biofilm permeability, detachment of biomass due to erosion, death of bacteria and production of biomass as nutrients are consumed.

Once the model equations are described in the tubular domain, we write the equations in a dimensionless form to observe the temporal and spatial scale that the terms depend on. For this, we introduce reference values of the spatial coordinates, time and other solution variables. In addition, we introduce the aspect ratio ϵ as the ratio of the aperture over the length of the tube.

The upscaling technique applied in this work is called homogenization. We assume that each variable can be written in an asymptotic expansion depending on ϵ. When the

aspect ratio ϵ approaches to zero, under some model assumptions, it is possible to reduce the dimensionality of the problem from three to one dimension.

The upscaled transport equation for the nutrients has the same form that is commonly used for the transport equation. As ϵ gets smaller, we obtain that the percentage of biofilm coverage area over time predicted by the pore-scale model approaches the one obtained using the effective equations, which shows a correspondence between both models. We observe that the derived effective quantities, in particular, the effective permeability depends on the pore geometry.

Inspired by the results of this work, the next step in this project is the work presented in Paper E, where we build a core-scale mathematical model for two-phase flow including reduction of permeability as a result of biomass.

Paper E: *Modeling of bio-plug technology: laboratory experiments and numerical simulations*

Up to 85% of oil remains in a reservoir after water injection. Then, enhanced oil recovery techniques are used in order to increase the oil production. Microbial enhanced oil recovery aims to improve the oil recovery using bacteria. Different bio products can be used for this purpose, e.g. gases and acids. The MEOR technology needs novel mathematical models for optimization of the outcomes. In this work we focus on the mathematical modeling of MEOR using the biomass.

The model includes water and oil, which are modeled by two mass conservation equations and multi-phase Darcy's law. We consider Brooks and Corey relations for the capillary pressure and relative permeabilities. There is only one nutrient injected in the system, which is modeled using the convection-diffusion equation. The model assumes an initial biofilm distribution. The processes included for the biofilm are consumption of nutrients, biofilm reproduction, biofilm decay and detachment due to shear forces. The biomass is modeled as a volume fraction of the REV changing over time which modifies the pore space from a clean porosity up to fill the pore. Then, we study the outcomes of different porosity-permeability relations and injection techniques.

Implementation of the mathematical model was done using the reservoir simulator MRST. One of the powerful tools in MRST is the automatic differentiation framework, which allows us to compute the Jabocian matrix. We use the existing functionality in MRST to adapt an accurate and efficient polymer simulator. Two-point flux approximation, backward Euler and Newton method are used to solve the system of equations.

Input data from single-phase flow experiments in a core sample is used to calibrate the mathematical model. The purpose of these experiments was to study the reduction of water injectivity due to biofilm growth. Using the estimated initial porosity and permeability of the core without biofilm, the core dimensions, an estimated of the initial biofilm after inoculation, the flux rate, the nutrient concentration and estimated parameters for the bacterium (growth factor, Monod half velocity, bacterial decay), we calibrate the stress coefficient.

After calibration, we run diverse numerical experiments to study the impact on the

mumerical results for different porosity-permeability relations in a core saturated with water and oil. We obtain that oil recovery depends on the selection of the porosity-permeability relation. We also perform numerical simulations to study different injectivity strategies to optimize the oil recovery and used resources. Following the work from Paper C, we perform a global sensitivity analysis to identify the critical model parameters. The Sobol sensitivity indices of the input parameters are computed based on uniform perturbation by $\pm$ 10% of the nominal parameter values [93].

In the same spirit of this core-scale model for the bio-plug technology, another MEOR effects and phenomena can be modeled such as interfacial tension reduction due to biosurfactants and the oil-water interfacial area, which is the research topic of Paper F.

Paper F: *Modeling and simulation of microbial enhanced oil recovery including interfacial area*

The novelty of this work is to include the role of the oil-water interfacial area (IFA) in enhanced oil recovery. The IFA allows us to model hysteresis in the capillary pressure in a physically consistent manner. In addition, the inclusion of IFA allows us to include in the model important microbial processes, such as production of surfactants on the IFA and the movement of bacteria towards the IFA.

The mathematical model includes two-phase flow (water and oil), oil-water interfacial area and transport of bacteria, nutrients and biosurfactants on the water phase. In contrast to Paper E, we do not consider biofilm formation on the rock walls. A balance equation derived by Niessner and Hassanizadeh [74] describes the evolution of IFA. We considered the relation between capillary pressure, water saturation and IFA given by Joekar-Niasar and Hassanizadeh [46]. The suspended bacteria in water die and consumes nutrients for reproduction and production of surfactants. The surfactants lower the oil-water interfacial tensions which, in turn, decreases the capillary pressure and the residual oil saturation. The movement of bacteria towards the IFA is modeled adding a velocity term in the transport equation of the bacteria given by the gradient of IFA times a diffusive parameter. The production of surfactants at the IFA is modeled adding an extra Monod-type function, i.e., we consider the production of surfactants as a function of both nutrient concentration and IFA given by the product of two Monod-type functions.

The mathematical model was implemented in a 2D rectangular domain in MATLAB. The two-phase flow equations were rewritten in the average pressure formulation, i.e., we solve the average pressure and the water saturation. The domain is discretized in an uniform cell-centered grid with half-cells at the boundaries. The two-point flux approximation and backward Euler are used for spatial and temporal discretization. The permeability on the cell faces is approximated by the harmonic mean, while for the rest of the parameters, we use the average values. We proposed a new linearization of the capillary pressure gradient, which depends on the water saturation and interfacial area. The iterative scheme used to solve the model equations consists of the following steps. First we solve the pressure equation using the previous values of water saturation and IFA, then we solve the saturation equation using the updated value of the pressure and

after we solve the IFA equation using the updated value of saturation. We iterate until the relative errors are smaller than a given tolerance (if there is no convergence after a given number of iterations, the time step is halved and the process is repeated). Once the errors are smaller than the tolerance, we solve the three transport equations until the relative error is smaller than the given tolerance. We update the IFT and compute the residual oil saturation reduction. We take the next time step and we repeat the procedure until the final time.

The domain dimensions, model parameters and initial and boundary conditions used for the numerical simulations were taken from diverse previous works. However, we observe that the results are physically incompatible, pointing that the existing experimental literature for MEOR and interfacial area was incomplete. We change the values of parameters to study different oil recovery profiles when we consider the effects of the IFA. We compared the oil recovery as a function of the pore volume injected for water flooding, MEOR not including IFA effects, MEOR including only the surfactant production on the interface, MEOR including only chemotaxis and MEOR including both effects (surfactant production at the interface and chemotaxis). The outcome of this simulation is that the oil recovery can be under- or overestimated if we do not include the IFA effects.

6.2 Conclusion

This thesis concerns mathematical modeling regarding biofilm formation at the pore and core scale. We proposed a pore-scale model inspired by laboratory experiments and derived effective quantities through homogenization. The upscaled quantities and equations are used to build a core-scale model for two-phase flow including biofilm formation. In particular, in this work we derived novel porosity-permeability relations including biofilm permeability and porosity.

So far it seems that the initial attachment of bacteria to the pore walls is a random process. One of the arising questions dealing with random systems is if there is a pattern to the randomness that can be characterized. Notwithstanding the random initial bacterial attachment, the coverage area of biofilm over time decreased as the flow rate increased, and using experimentally determined parameters, we obtained a good match to the data and numerical simulations.

Modeling of systems require estimation of parameters. These parameters depend on several factors, e.g., water activity, temperature and acidity change the value of maximum bacterial growth rate. It is expensive and time consuming to estimate parameters and different experiments need to be performed to measure various parameters. For example, to estimate the biofilm composition at a given time it is necessary to break the tube to extract a sample of biofilm and observe it in the microscope. Therefore, it is common to perform a global sensitivity analysis to quantify the effect of variability or uncertainty in the model parameters that are assumed to be sensitive with respect to variation in an objective value, the biofilm coverage area and the oil recovery in our study. Based on the numerical sensitivity study at the pore scale, the true value of each of the

model parameters must be estimated with sufficient accuracy to lead to a reliable estimate of the biofilm area. This is a beautiful tragedy, confirming the difficulty of this problem.

Another big issue dealing with microbial enhanced oil recovery is the significant attachment of bacteria in the inlet. Injection of nutrients through the same side leads to a faster formation of biofilm in the inlet and possibly clogging. We capture this behavior in the numerical simulations. Recalling the strong dependence of biofilm growth on temperature, then one strategy to avoid clogging in the inlet is to modify the temperature in the inlet to reduce biofilm formation.

In this research we studied different mathematical models for biofilm at the pore and core scale. Throughout this thesis we aimed to describe the process of deriving upscaled mathematical models from pore-scale models. The numerical solution of these models, calibration of parameters and sensitivity analysis techniques are also discussed. The stress coefficients for two different bacterial species using data from pore- and core-scale experiments were calibrated. Input parameters for mathematical models and diverse measurements from the performed laboratory experiments can be found in this work.

6.3 Outlook

Inspired by this work, there is further and more interesting work to be done. One of the challenges faced in this project was the repetition of the experiments in the pore scale to confirm that the results were reliable. It is known that the attachment of bacteria is strongly dependent on the surface conditions. In the laboratory, the microchannel was cleaned after finalizing the experiment in order to reuse it for a following experiment. Then, we suspect that the washing procedure altered the surface properties of the microchannel which leaded to different initial attachment. Therefore, it is important to improve the experimental setup to get comparable initial conditions.

Regarding the pore-scale experiments, future experiments in perforated domains have been planned to estimate biofilm permeability, comparing the water flux profile of a clean micromodel to the micromodel with biofilm. The pore-scale mathematical model presented in Sec. 2.2 will be used to perform this comparison. The numerical solution of this mathematical model is challenging because of the moving interface between the water and biofilm, which is modeled using a phase field formulation. Then, advanced numerical methods are needed to perform numerical simulations.

In Paper D we upscaled the pore-scale mathematical model for permeable multicomponent biofilm in a thin channel and tube, assuming that convection and diffusion happen at the same time scale. Investigating other regimes where transport or reaction dominate diffusion will lead to different effective models.

In Sec. 3.2 we presented the derivation of the Darcy's law in a perforated domain. Using similar techniques, it is possible to derive effective equations upscaling the mathematical model presented in Sec. 2.2. Then, we could use the framework of two-scale convergence to prove the existence and uniqueness of the macroscopic solution in the

limit as ϵ approaches zero. In addition, we could compare the numerical outcome of the pore-scale and upscaled model to verify that the upscaled model approaches to the average behavior of the original model equations.

Through our research, we hope to convince the community of the importance of including more complex phenomena in MEOR simulation, e.g., biofilm permeability, biofilm composition, IFA and chemotaxis and to inspire further experiments focusing on these relevant effects.

Bibliography

[1] Aavatsmark, I. (2002). An introduction to multipoint flux approximations for quadrilateral grids. *Computational Geosciences 6*(3), 405–432. doi: 10.1023/A:1021291114475.

[2] Ahmad, I. and Husain, F. M. (2017). Biofilms in plant and soil health. John Wiley & Sons Ltd. ISBN 9781119246343. doi: 10.1002/9783527627967.

[3] Aksoy, A. (2015). Numerical models | Parameter estimation. In North, G. R., Pyle, J., and Zhang, F. (editors), *Encyclopedia of Atmospheric Sciences*, pages 181 – 186. Academic Press, Oxford, second edition. doi: 10.1016/B978-0-12-382225-3.00494-1.

[4] Alpkvist, E. and Klapper, I. (2007). A multidimensional multispecies continuum model for heterogeneous biofilm development. *Bulletin of Mathematical Biology 69*, 765–789. doi: 10.1.1/jpb001.

[5] Amann, R. and Rosselló-Móra, R. (2016). After all, only millions? *mBio 7*(4). doi: 10.1128/mBio.00999-16.

[6] Ansorge, R. and Sonar, T. (2009). Mathematical models of fluid dynamics: modeling, theory, basic numerical facts - An introduction, second edition. Wiley-VCH Verlag GmbH & Co. KGaA, United States. ISBN 9783527407743. doi: 10.1002/9783527627967.

[7] Atkinson, S. and Williams, P. (2009). Quorum sensing and social networking in the microbial world. *Journal of The Royal Society Interface 6*(40), 959–978. doi: 10.1098/rsif.2009.0203.

[8] Auriault, J., Boutin, C., and Geindreau, C. (2010). Homogenization of coupled phenomena in heterogenous media. ISTE Ltd and John Wiley & Sons, Inc., Great Britain. ISBN 9781848211612. doi: 10.1002/9780470612033.

[9] Bazin, M. J. and Prosser, J. I. (2018). Physiological models in microbiology: Volume II. CRC Press, United States. ISBN 0849359554. doi: 10.1201/9781351075640.

[10] Bear, J. (1972). Dynamics of fluids in porous media. Elsevier Science, New York.

[11] Beavers, G. S. and Joseph, D. D. (1967). Boundary conditions at a naturally permeable wall. *Journal of Fluid Mechanics 30*(1), 197—207. doi: 10.1017/S0022112067001375.

[12] Bennett, T. (2012). Transport by advection and diffusion. Wiley Global Education, United Kingdom. ISBN 9781118476758.

[13] Berthelot, R. and Neethirajan, S. (2017). Harnessing electrical energy for anti-biofilm therapies: effects of current on cell morphology and motility. *Journal of Experimental Nanoscience 12*(1), 197–207. doi: 10.1080/17458080.2017.1296977.

[14] Bitton, G. (2005). Wasterwater microbiology, 3rd edition. John Wiley & Sons, United States. ISBN 9780471650713. doi: 10.1002/0471717967.

[15] Bjarnsholt, T. (2013). The role of bacterial biofilms in chronic infections. *APMIS 121*(s136), 1–58. doi: 10.1111/apm.12099.

[16] Bringedal, C. (2015). Modeling of heat transfer in porous media in the context of geothermal energy extraction. Ph.D. thesis, University of Bergen.

[17] Bringedal, C., Berre, I., Pop, I. S., and Radu, F. A. (2015). A model for non-isothermal flow and mineral precipitation and dissolution in a thin strip. *Journal of Computational and Applied Mathematics 289*, 346–355. doi: 10.1016/j.cam.2014.12.009.

[18] Bringedal, C., Berre, I., Pop, I. S., and Radu, F. A. (2016). Upscaling of non-isothermal reactive porous media flow with changing porosity. *Transport in Porous Media 114*(2), 371–393. doi: 10.1007/s11242-015-0530-9.

[19] Brun, K., M, Berre, I., Nordbotten, J. M., and Radu, F. A. (2018). Upscaling of the coupling of hydromechanical and thermal processes in a quasi-static poroelastic medium. *Transport in Porous Media 124*(1), 137–158. doi: 10.1007/s11242-018-1056-8.

[20] Bryant, S. L. and Lockhart, T. P. (2002). Reservoir engineering analysis of microbial enhanced oil recovery. *Society of Petroleum Engineers 5*(5), 365–374. doi: 10.2118/79719-PA.

[21] Carrera, J. (1992). Methodological conceptualization of mathematical modelling. *Mathematical and Computer Modelling 16*(12), 19–28. doi: 10.1016/0895-7177(92)90015-D.

[22] Chaillan, F., Le Flèche, A., Bury, E., Phantavong, Y. H., Grimont, P., Saliot, A., and Oudot, J. (2004). Identification and biodegradation potential

of tropical aerobic hydrocarbon-degrading microorganisms. *Research in Microbiology 155*(7), 587–595. doi: 10.1016/j.resmic.2004.04.006.

[23] Chen-Charpentier, B. M., Dimitrov, D. T., and Kojouharov, H. V. (2009). Numerical simulation of multi-species biofilms in porous media for different kinetics. *Mathematics and Computers in Simulation 79*, 1846–1861. doi: 10.1016/j.matcom.2007.03.002.

[24] Cioranescu, D. and Donato, P. (1999). An Introduction to Homogenization. Oxford Lecture Series in Mathe. Oxford University Press, Great Britain. ISBN 9780198565543.

[25] COMSOL Multiphysics® (2015). v. 5.2. COMSOL AB. www.comsol.com., Stockholm, Sweden.

[26] Deng, W., Bayani Cardenas, M., Kirk, M. F., Altman, S. J., and Bennett, P. C. (2013). Effect of permeable biofilm on micro–and macro–scale flow and transport in bioclogged pores. *Environmental Science and Technology 47*, 11092–11098. doi: 10.1021/es402596v.

[27] Dí-az, M., Castro, M., Copaja, S., and Guiliani, N. (2018). Biofilm formation by the acidophile bacterium *Acidithiobacillus thiooxidans* involves c-di-GMP pathway and pel exopolysaccharide. *Genes 9*, 113. doi: 10.3390/genes9020113.

[28] Donea, J., Huerta, A., Ponthot, J.-P., and Rodrí-guez-Ferran, A. (2004). Arbitrary Lagrangian–Eulerian methods. In Stein, E., de B., R., and Hughes, T. J. R. (editors), *Encyclopedia of Computational Mechanics*, chapter 14. American Cancer Society. doi: 10.1002/0470091355.ecm009.

[29] Duddu, R., Chopp, D. L., and Moran, B. (2009). A two-dimensional continuum model of biofilm growth incorporating fluid flow and shear stress based detachment. *Biotechnology and Bioengineering 103*(1), 92–104. doi: 10.1002/bit.22233.

[30] Dumitrache, C. and Petrache, A. (2012). Interface condition for the coupling of a fluid and porous media. *Acta Technica Napocensis - Series: Applied Mathematics, Mechanics, and Engineering 55*(2), 1221–5872. doi: 10.1002/bit.22233.

[31] Dykhuizen, D. (2005). Species numbers in bacteria. *Proceedings. California Academy of Sciences 56*(6 Suppl 1), 62–71. doi: 10.3390/genes9020113.

[32] Eck, C., Garcke, H., and Knabner, P. (2017). Mathematical modeling. Springer. ISBN 978-3-319-55160-9.

[33] Fasano, A. and Primicerio, M. (1983). Free boundary problems: Theory and applications, Vol. II. Pitman, Boston.

[34] Fujiwara, K., Sugai, Y., Yazawa, N., Ohno, K., Hong, C. X., and Enomoto, H. (2004). Chapter 15 Biotechnological approach for development of microbial enhanced oil recovery technique. In Vazquez-Duhalt, R. and Quintero-Ramirez, R. (editors), *Petroleum Biotechnology*, volume 151 of *Studies in Surface Science and Catalysis*, pages 405–445. Elsevier. doi: 10.1016/S0167-2991(04)80156-3.

[35] Galántai, A. (2000). The theory of Newton's method. *Journal of Computational and Applied Mathematics 124*(1), 25 – 44. doi: 10.1016/S0377-0427(00)00435-0.

[36] Gibou, F., Fedkiw, R., and Osher, S. (2018). A review of level-set methods and some recent applications. *Journal of Computational Physics 353*, 82–109. doi: 10.1016/j.jcp.2017.10.006.

[37] Goudar, C. T. and Devlin, J. F. (2001). Nonlinear estimation of microbial and enzyme kinetic parameters from progress curve data. *Water Environment Research 73*(3), 260–265.

[38] Guo, H., Dou, M., Hanqing, W., and et al. (2017). Proper use of capillary number in chemical flooding. *Journal of Chemistry 2017*, Article ID 4307368. doi: 10.1155/2017/4307368.

[39] Hamby, D. M. (1994). A review of techniques for parameter sensitivity analysis of environmental models. *Environmental Monitoring and Assessment 32*(2), 135–154. doi: 10.1007/BF00547132.

[40] Hendry, M. J., Lawrence, J. R., and Maloszewski, P. (1997). The role of sorption in the transport of *Klebsiella oxytoca* through saturated silica sand. *Groundwater 35*(4), 574–584. doi: 10.1111/j.1745-6584.1997.tb00122.x.

[41] Holm, R. (2009). Modeling of three-phase flow functions for applications in enchanced oil recovery. Ph.D. thesis, University of Bergen.

[42] Hommel, J., Coltman, E., and Class, H. (2018). Porosity–permeability relations for evolving pore space: A review with a focus on (bio-)geochemically altered porous media. *Transport in Porous Media 124*(2), 589–629. doi: 10.1007/s11242-018-1086-2.

[43] Horn, H. and Lackner, S. (2014). Modeling of biofilm systems: A review. *Advances in Biochemical Engineering/Biotechnology 146*, 53–76. doi: 10.1007/10_2014_275.

[44] Hornung, U. (1997). Homogenization and porous media. Springer, United States. ISBN 978-1-4612-7339-4. doi: 10.1007/978-1-4612-1920-0.

[45] Jefferson, K. K. (2004). What drives bacteria to produce a biofilm? *FEMS Microbiology Letters 236*(2), 163–173. doi: 10.1111/j.1574-6968.2004.tb09643.x.

[46] Joekar-Niasar, V. and Hassanizadeh, S. M. (2012). Uniqueness of specific interfacial area–capillary pressure–saturation relationship under non-equilibrium conditions in two-phase porous media flow. *Transport in Porous Media 94*(2), 465–486. doi: 10.1007/s11242-012-9958-3.

[47] Johnson, C. (1987). Numerical solution of partial differential equations by the finite element method. Studentlitteratur, Lund, Sweden.

[48] Karambeigi, M. S., Schaffie, M., and Fazaelipoor, M. H. (2013). Improvement of water flooding efficiency using mixed culture of microorganisms in heterogeneous micro-models. *Petroleum Science and Technology 31*(9), 923–931. doi: 10.1080/10916466.2010.506461.

[49] Khan, M. R., Baranitharan, E., Prasad, D. M. R., and Cheng, C. K. (2016). Fast biofilm formation and its role on power generation in palm oil mill effluent fed microbial fuel cell. *MATEC Web of Conferences 62*, 04002. doi: 10.1051/matecconf/20166204002.

[50] Kim, S.-B. (2006). Numerical analysis of bacterial transport in saturated porous media. *Hydrological Processes 20*(5), 1177–1186. doi: 10.1002/hyp.5930.

[51] Krell, T., Lacal, J., Muñoz Martí-nez, F., Reyes-Darias, J. A., Cadirci, B. H., Garcí-a-Fontana, C., and Ramos, J. L. (2011). Diversity at its best: bacterial taxis. *Environmental Microbiology 13*(5), 1115–1124. doi: 10.1111/j.1462-2920.2010.02383.x.

[52] Krogstad, S., Lie, K.-A., Møyner, O., Nilsen, H. M., and Raynaud, X. (2015). MRST-AD - an open-source framework for rapid prototyping and evaluation of reservoir simulation problems. In *ANSS 2015*. doi: 10.2118/173317-MS.

[53] Kumar, K., van Noorden, T., and Pop, I. S. (2011). Effective dispersion equations for reactive flows involving free boundaries at the microscale. *Multiscale Modeling & Simulation 9*(1), 29–58. doi: 10.1137/100804553.

[54] Landa-Marbán, D. (2016). Modeling and simulation of microbial enhanced oil recovery: A new approach which includes the role of interfacial area. Master's thesis, University of Bergen, Norway.

[55] Landa-Marbán, D., Liu, N., Pop, I. S., Kumar, K., Pettersson, P., Bødtker, G., Skauge, T., and Radu, F. A. (2018). A pore-scale model for permeable biofilm: Numerical simulations and laboratory experiments. *Transport in Porous Media 127*(3), 643–660. doi: 10.1007/s11242-018-1218-8.

[56] Landa-Marbán, D., Pop, I. S., Kumar, K., and Radu, F. A. (2019). Numerical simulation of biofilm formation in a microchannel. In Radu, F. A., Kumar, K., Berre, I., Nordbotten, J. M., and Pop, I. S. (editors), *Numerical Mathematics and Advanced Applications ENUMATH 2017*, volume 126, pages 799–807. Springer, Cham. doi: 10.1007/978-3-319-96415-7_75.

[57] Landa-Marbán, D., Radu, F. A., and Nordbotten, J. M. (2017). Modeling and simulation of microbial enhanced oil recovery including interfacial area. *Transport in Porous Media 120*(2), 395–413. doi: 10.1007/s11242-017-0929-6.

[58] Langer, J. S. (1986). Models of pattern formation in first-order phase transitions. In Grinstein, G. and Mazenko, G. (editors), *Directions in Condensed Matter Physics*, Series on Directions in Condensed Matter Physics, pages 165 –186. World Scientific. doi: 10.1142/9789814415309_0005.

[59] Lie, K.-A. (2016). An introduction to reservoir simulation using MATLAB: User guide for the MATLAB reservoir simulation toolbox (MRST). SINTEF ICT.

[60] Lindley, B., Wang, Q., and Zhang, T. (2011). A multicomponent model for biofilm-drug interaction. *Discrete & Continuous Dynamical Systems - B 15*(2), 417. doi: 10.3934/dcdsb.2011.15.417.

[61] List, F. and Radu, F. A. (2016). A study on iterative methods for solving Richards' equation. *Computational Geosciences 20*(2), 341–353. doi: 10.1007/s10596-016-9566-3.

[62] Liu, N., Skauge, T., Landa-Marbán, D., Hovland, B., Thorbjørnsen, B., Radu, F. A., Vik, B. F., Baumann, T., and Bødtker, G. (2019). Microfluidic study of effects of flow velocity and nutrient concentration on biofilm accumulation and adhesive strength in the flowing and no-flowing microchannels. *Journal of Industrial Microbiology & Biotechnology* doi: 10.1007/s10295-019-02161-x.

[63] Long-Qing, C. (2002). Phase-field models for microstructure evolution. *Annual Review of Materials Research 32*(1), 113–140. doi: 10.1146/annurev.matsci.32.112001.132041.

[64] Marsh, P. D. (2006). Dental plaque as a biofilm and a microbial community - implications for health and disease. *BMC Oral Health 6*(Suppl 1), S14. doi: 10.1186/1472-6831-6-S1-S14.

[65] Mikelić, A., Wheeler, M. F., and Wick, T. (2015). Phase-field modeling of a fluid-driven fracture in a poroelastic medium. *Computational Geosciences 19*(6), 1171–1195. doi: 10.1007/s10596-015-9532-5.

[66] Morgenroth, E. and Wilderer, P. A. (2000). Influence of detachment mechanisms on competition in biofilms. *Water Research 34*(2), 417–426. doi: 10.1016/S0043-1354(99)00157-8.

[67] Murphy, E. M. and Ginn, T. R. (2000). Modeling microbial processes in porous media. *Hydrogeology Journal 8*(1), 142–158. doi: 10.1007/s100409900043.

[68] Muskat, M. (1934). The flow of compressible fluids through porous media and some problems in heat conduction. *Physics 5*(3), 71–94. doi: 10.1063/1.1745233.

[69] Nagalakshmi, T., Karthikeshwaran, R., Mascarenhas, J., and Nascimento Bernardo, M. (2014). A study of *Clostridium tryobutyricum* in carbonate reservoir for microbial enhanced oil recovery. *Indian Journal Of Science And Technology 7*(S6), 68–73. doi: 10.17485/ijst/2014/v7iS6/61411.

[70] Naji, K. M., Abdullah, Q. Y. M., AL-Zaqri, A. Q. M., and Alghalibi, S. M. (2014). Evaluating the biodeterioration enzymatic activities of fungal contamination isolated from some ancient yemeni mummies preserved in the national museum. *Biochemistry Research International 2014*, 1–9. doi: 10.1155/2014/481508.

[71] Nambi, I. M., Werth, C. J., Sanford, R. A., and Valocchi, A. J. (2003). Pore-scale analysis of anaerobic halorespiring bacterial growth along the transverse mixing zone of an etched silicon pore network. *Environmental Science & Technology 37*(24), 5617–5624. doi: 10.1021/es034271w.

[72] Neuweiler, I. and Vogel, H.-J. (2007). Upscaling for unsaturated flow for non-Gaussian heterogeneous porous media. *Water Resources Research 43*(3), W03443. doi: 10.1029/2005WR004771.

[73] Nielsen, S. M., Nesterov, I., and Shapiro, A. A. (2016). Microbial enhanced oil recovery—a modeling study of the potential of spore-forming bacteria. *Computational Geosciences 20*(3), 567–580. doi: 10.1007/s10596-015-9526-3.

[74] Niessner, J. and Hassanizadeh, S. M. (2008). A model for two-phase flow in porous media including fluid-fluid interfacial area. *Water Resources Research 44*(8), W08439. doi: 10.1029/2007WR006721.

[75] Nordbotten, J. M. and Celia, M. A. (2011). Geological storage of CO2: Modeling approaches for large-scale simulation. John Wiley & Sons. doi: 10.1002/9781118137086.

[76] Nourzadeh, N., Shadizadeh, S. R., and Manshad, A. K. (2017). Determination of pore size distribution profile along wellbore: using repeat formation tester. *Journal of Petroleum Exploration and Production Technology 7*(3), 621–626. doi: 10.1007/s13202-016-0310-2.

[77] Osher, S. and Sethian, J. A. (1988). Fronts propagating with curvature-dependent speed: Algorithms based on Hamilton-Jacobi formulations. *Journal of Computational Physics 79*(1), 12 – 49. doi: 10.1016/0021-9991(88)90002-2.

[78] Paniconi, C. and Putti, M. (1994). A comparison of Picard and Newton iteration in the numerical solution of multidimensional variably saturated flow problems. *Water Resources Research 30*(12), 3357–3374. doi: 10.1029/94WR02046.

[79] Pavlovskaya, G. E., Meersmann, T., Jin, C., and Rigby, S. P. (2018). Fluid flow in a porous medium with transverse permeability discontinuity. *Phys. Rev. Fluids 3*, 044102. doi: 10.1103/PhysRevFluids.3.044102.

[80] Percival, S. L., Suleman, L., Vuotto, C., and Donelli, G. (2015). Healthcare-associated infections, medical devices and biofilms: risk, tolerance and control. *Journal of Medical Microbiology 64*, 323—334. doi: 10.1099/jmm.0.000032.

[81] Peszynska, M., Trykozko, A., Iltis, G., Steffen, S., and Wildenschild, D. (2016). Biofilm growth in porous media: Experiments, computational modeling at the porescale, and upscaling. *Advances in Water Resources 95*, 288–301. doi: 10.1016/j.advwatres.2015.07.008.

[82] Petrovich, M., Wu, C.-Y., Rosenthal, A., Chen, K.-F., Packman, A. I., and Wells, G. F. (2017). Nitrosomonas europaea biofilm formation is enhanced by *Pseudomonas aeruginosa*. *FEMS microbiology ecology 93*(5). doi: 10.1093/femsec/fix047.

[83] Picioreanu, C., Kreft, J. U., and Van Loosdrecht, M. C. (2004). Particle-based multidimensional multispecies biofilm model. *Applied and Environmental Microbiology 70*(5), 3024–3040. doi: 10.1128/AEM.70.5.3024-3040.2004.

[84] Radu, F. A., Nordbotten, J. M., Pop, I. S., and Kumar, K. (2015). A robust linearization scheme for finite volume based discretizations for simulation of two-phase flow in porous media. *Journal of Computational and Applied Mathematics 289*, 134 – 141. doi: 10.1016/j.cam.2015.02.051.

[85] Rohde, C., Redeker, M., and Pop, I. S. (2016). Upscaling of a tri-phase phase-field model for precipitation in porous media. *IMA Journal of Applied Mathematics 81*(5), 898–939. doi: 10.1093/imamat/hxw023.

[86] Sandvin, A., Nordbotten, J. M., and Aavatsmark, I. (2011). Multiscale mass conservative domain decomposition preconditioners for elliptic problems on irregular grids. *Computational Geosciences 15*(3), 587–602. doi: 10.1007/s10596-011-9226-6.

[87] Scheffers, D. J. (2013). Bacterial reproduction and growth. In *eLS*. American Cancer Society. ISBN 9780470015902. doi: 10.1002/9780470015902.a0001419.pub2.

[88] Schulz, R. (2019). Biofilm modeling in evolving porous media with Beavers-Joseph condition. *ZAMM - Journal of Applied Mathematics and Mechanics / Zeitschrift für Angewandte Mathematik und Mechanik* page e201800123. doi: 10.1002/zamm.201800123.

[89] Schulz, R. and Knabner, P. (2016). Derivation and analysis of an effective model for biofilm growth in evolving porous media. *Mathematical Methods in the Applied Sciences 40*(8), 2930–2948. doi: 10.1002/mma.4211.

[90] Sen, R. (2008). Biotechnology in petroleum recovery: The microbial EOR. *Progress in Energy and Combustion Science 34*(6), 714–724. doi: 10.1016/j.pecs.2008.05.001.

[91] Shehata, T. E. and Marr, A. G. (1971). Effect of nutrient concentration on the growth of *Escherichia coli*. *Journal of Bacteriology 107*(1), 210–216.

[92] Shuler, M. L. and Kargi, F. (2002). Bioprocess engineering: Basic concepts. Prentice Hall PTR, Upper Saddle River, New Jersey.

[93] Sobol, I. M. (2001). Global sensitivity indices for nonlinear mathematical models and their Monte Carlo estimates. *Mathematics and Computers in Simulation 55*(1), 271 – 280. doi: 10.1016/S0378-4754(00)00270-6.

[94] Suthar, H., Hingurao, K., Desai, A., and Nerurkar, A. (2009). Selective plugging strategy-based microbial-enhanced oil recovery using *Bacillus licheniformis* TT33. *Journal of Microbiology and Biotechnology 19*(10), 1230–1237. doi: 10.4014/jmb.0904.04043.

[95] Taylor, S. W. and Jaffé, P. R. (1990). Substrate and biomass transport in a porous medium. *Water Resources Research 26*(9), 2181–2194. doi: 10.1029/WR026i009p02181.

[96] Tierra, G., Pavissich, J. P., Nerenberg, R., Xu, Z., and Alber, M. S. (2015). Multicomponent model of deformation and detachment of a biofilm under fluid flow. *Journal of The Royal Society Interface 12*(106), 20150045. doi: 10.1098/rsif.2015.0045.

[97] Toyofuko, M., Inaba, T., Kiyokawa, T., Obana, N., Yawata, Y., and Nomura, N. (2016). Environmental factors that shape biofilm formation. *Bioscience, Biotechnology, and Biochemistry 80*(1), 7–12. doi: 10.1080/09168451.2015.1058701.

[98] Valiei, A., Kumar, A., Mukherjee, P. P., Liu, Y., and Thundat, T. (2012). A web of streamers: biofilm formation in a porous microfluidic device. *Lab Chip 12*(24), 5133–5137. doi: 10.1039/C2LC40815E.

[99] van Noorden, T. L. (2008). Crystal precipitation and dissolution in a porous medium: Effective equations and numerical experiments. *Multiscale Modeling & Simulation 7*(3), 1220–1236. doi: 10.1137/080722096.

[100] van Noorden, T. L., Pop, I. S., Ebigbo, A., and Helmig, R. (2010). An upscaled model for biofilm growth in a thin strip. *Water Resources Research 46*(6), W06505. doi: 10.1029/2009WR008217.

[101] Vu, B., Chen, M., Crawford, R. J., and Ivanova, E. P. (2009). Bacterial extracellular polysaccharides involved in biofilm formation. *Molecules 14*(7), 2535–2554. doi: 10.3390/molecules14072535.

[102] Wang, Q. and Zhang, T. (2010). Review of mathematical models for biofilms. *Solid State Communications 150*(21), 1009 – 1022. doi: 10.1016/j.ssc.2010.01.021.

[103] Wang, X., Wang, G., and Hao, M. (2015). Modeling of the *Bacillus subtilis* bacterial biofilm growing on an agar substrate. *Computational and Mathematical Methods in Medicine 2015*, 581829. doi: 10.1155/2015/581829.

[104] Webb, H. K., Crawford, R. J., Sawabe, T., and Ivanova, E. P. (2009). Poly(ethylene terephthalate) polymer surfaces as a substrate for bacterial attachment and biofilm formation. *Microbes and Environments 24*(1), 39–42. doi: 10.1264/jsme2.ME08538.

[105] Wolfram, S. (1984). Cellular automata as models of complexity. *Nature 311*, 419–424. doi: 10.1038/311419a0.

[106] Wood, D. A. (2019). Microbial improved and enhanced oil recovery (MIEOR): Review of a set of technologies diversifying their applications. *Advances in Geo-Energy Research 3*(2), 122–140. doi: 10.26804/ager.2019.02.02.

[107] Yang, J., Wang, X., Zou, H., and Liang, G. (2010). A Combined finite-element and finite-volume method in reservoir simulation. In *2010 Second World Congress on Software Engineering*, volume 2, pages 325–328. doi: 10.1109/WCSE.2010.126.

[108] Yarbrough, H. F. and Coty, V. F. (1983). Microbial enhanced oil recovery from the upper crustaceous nacatoch formation. In *International Conference on Microbial Enhancement of Oil Recovery*.

[109] Zhang, M., Jiang, S., Tanuwidjaja, D., Voutchkov, N., Hoek, E. M. V., and Cai, B. (2011). Composition and variability of biofouling organisms in seawater reverse osmosis desalination plants. *Applied and Environmental Microbiology 77*(13), 4390–4398. doi: 10.1128/AEM.00122-11.

[110] Zhang, T., Cogan, N., and Wang, Q. (2008). Phase field models for biofilms. I. Theory and one-dimensional simulations. *SIAM Journal on Applied Mathematics 69*(3), 641–669. doi: 10.1137/070691966.

Part II

Scientific Results

Graphic design: Communication Division, UiB / Print: Skipnes Kommunikasjon AS

uib.no

ISBN: 978-82-308-3004-8